Soil Dynamics and Earthquake Engineering 124 (2019) 16–34

Contents lists available at ScienceDirect

Soil Dynamics and Earthquake Engineering

journal homepage: www.elsevier.com/locate/soildyn

Performance assessment of the Greater Tehran Area buried gas distribution pipeline network under liquefaction

Dan (Danesh) Nourzadeh[a,*], Pedram Mortazavi[b,1], Abbas Ghalandarzadeh[c], Shiro Takada[d], Mohammad Ahmadi[c]

[a] Ontario Power Generation (OPG), Toronto, Canada
[b] J. L. Richards and Associates Limited, Ottawa, Canada
[c] School of Civil Engineering, University College of Engineering, University of Tehran, Tehran, Iran
[d] Earthquake Disaster Mitigation Non-for-Profit Organization, Kobe, Japan

ARTICLE INFO

Keywords:
Liquefaction
Soil-structure interaction
Buried pipeline
Risk assessment

ABSTRACT

The interconnectedness of current urban life with infrastructures urges the decision-makers to consider the resilience of urban lifeline systems as a priority. This motivates the research presented here, where the performance of a complex urban gas distribution system in a city with more than 12 million resident population is evaluated under the effects of seismic-induced liquefaction. The paper reviews the liquefaction potential in the Greater Tehran Area, and identifies the inputs for the analysis of soil-pipe interactions. The performance assessment is carried out using both numerical (finite elements analysis) and small scaled experimental assessments, for validation of the numerical models. The experimental results indicate that the numerical models are adequate for the performance evaluation of buried pipelines. The assessment shows that the buried pipelines perform well in most areas of the city, however, structural damage is expected in areas with higher seismic demands. In such areas, hands-on countermeasures are proposed to mitigate the risk of liquefaction-induced damage on the buried pipelines system. The results, methodology and procedures can be used as a framework the similar urban infrastructure risk analysis and mitigation studies.

1. Introduction

1.1. Background and motivation

Pipelines are among the most important lifelines in urban and metropolitan areas. Depending on their function, pipeline networks prevalently consist of reinforced concrete, steel, or polyethylene (PE) pipes. Pipeline systems are used for various purposes, including transmission, or distribution of gas, clean water, waste water, etc. Such distribution systems commonly consist of a network of buried pipelines, which are susceptible to structural damage during seismic events. In fact, in seismically active regions, earthquakes can be regarded as the most destructive natural hazard to buried pipelines.

The dependence of the general public on continuous operation of buried pipelines makes structural damage to these lifelines following major earthquakes a public safety concern in large cities. Further, structural damage to buried pipelines used for the distribution of combustible, flammable, and/or toxic gases can lead to major secondary catastrophes. The severity of such risks and consequences are much greater in larger cities and would, therefore, require special consideration and risk mitigation by the stakeholders and the decision-making authorities.

Given the vulnerability of gas distribution pipelines to seismic events, the socioeconomic importance of their operation, and the post-hazard risks associated with structural damage to these networks, it is of great importance to identify the critical seismic mechanisms that can cause structural damage to the pipeline networks, assess their seismic performance in large cities, and mitigate their potential risk and damage. Previous studies on the performance of pipeline networks in large metropolitan areas include [1–10]. Destructive seismic mechanisms to buried pipelines, based on the various geological parameters include seismic wave propagation effects and the induced permanent ground deformations (PGDs), which can be caused by liquefaction, faulting, and landslide.

* Corresponding author.
E-mail addresses: danesh.nourzadeh@opg.com, Danesh.nourzadeh@carleton.cam (D.D. Nourzadeh), pedram.mortazavi@mail.utoronto.ca (P. Mortazavi), aghaland@ut.ac.ir (A. Ghalandarzadeh), takada_smartinfra@kobe.zaq.jp (S. Takada), moh.ahmadi@ut.ac.ir (M. Ahmadi).
[1] Currently at Department of Civil and Mineral Engineering, University of Toronto, Toronto, Canada.

https://doi.org/10.1016/j.soildyn.2019.05.033
Received 20 October 2018; Received in revised form 20 April 2019; Accepted 20 May 2019
0267-7261/ © 2019 Elsevier Ltd. All rights reserved.

1.2. Effect of liquefaction on buried pipelines

Saturated or partially saturated loose sandy soils are prone to liquefaction during seismic events. Earthquake excitations rapidly increase the pore water pressures in each loading cycle. If the increased water pressure exceeds the contact stresses between the soil grains, the soil will become liquefied. In such a state where the effective soil contact stress is zero, the soil grains lose their contact and soil acts similar to a viscous liquid with a density equal to that of the saturated soil specific weight. The occurrence of liquefaction will result in large permanent ground displacements (PGDs) which will continue until the pore water has drained and the effective contact stress becomes positive.

The overall performance of oil and gas pipelines during past earthquakes has been satisfactory; however, catastrophic events have also occurred in some cases mostly due to poor soil conditions and instabilities. Among these cases of soil failure, liquefaction in loose sandy soils with high groundwater level has been a major cause of damage. Hence, liquefaction can have destructive effects on buried pipelines and can be regarded as a potential source of disruption in buried pipelines. O'Rourke et al. [11–14] have noted that more than half of the failures in buried pipelines in the 1906 San Francisco earthquake was due to lateral spreading caused by liquefaction. Studying the 1906 San Francisco and 1989 Loma Prieta earthquakes has shown that liquefaction induced damage is directly proportional to peak ground displacement (PGD). During the 1995 Kobe earthquake buried water pipelines underwent significant damage, reporting more than 4000 cases in the overall area subjected to ground shaking [15].

Liquefaction can cause damage in buried structures with different mechanisms. Some of these mechanisms include reduction of soil bearing forces, imposed buoyancy forces when the structure is submerged in the liquefied area of the soil [16,17], ground settlements, and lateral flow of the soil, which is known as lateral spreading. Lateral spreading occurs in slopes less than 5°. Towhata et al. [18] observed that lateral spreading is accompanied by vertical movements as well. The liquefaction-induced damage in buried pipelines can be caused by each of these mechanisms based on different factors such as soil properties, soil shear stress capacity, location of the pipe, the topology of the liquefied area, and the level and duration of ground motion. In addition, the direction of ground movement relative to the direction of the pipeline is of importance. For instance, under longitudinal permanent ground displacements (PGD), the pipeline experiences tension and compression at different locations [19]. For lateral PGDs, the pipeline is likely to experience mostly bending. Connection failures such as weld fracture and bolt failure could occur under these actions if the pipe is not properly designed and detailed. However, as noted by O'Rouke et a. [20], when the pipelines are detailed properly, using high-quality welds, both the pipe section and the welded connections will have inherent ductility. The performance of the pipelines depends on pipe material as well. O'Rouke et a. [20] indicate that high- and medium-density PE pipes can sustain high tensile strains before fracture.

In order to ensure a satisfactory performance of buried pipelines in liquefaction, other than careful detailing for seismic demands, real-time monitoring and consistent field investigations are required. The general approach for liquefaction risk mitigation, in large urban areas, is to limit the losses by risk management. However, in more isolated areas, hazard elimination could be considered by means of soil rehabilitations, compaction, or other soil reinforcement methods [21–24].

1.3. Performance assessment methods

Several methods can be used for performance assessment of buried pipelines in liquefaction. One of the common methods is using the traditional fragility curves [25]. In this method, location of the pipeline is specified. Next, performance level and the importance factor for the pipe are determined. Afterwards, the hazard level is determined in terms of PGD and PGV. The assessment can then be carried out using charts, tables, and fragility curves that are derived based on empirical data. Simplified methods have been developed and proposed for the performance assessment of buried pipelines in liquefaction in many studies [26–33]. One of such methods, is the equivalent static method (ESM), adopted and described in many seismic design guidelines and studies [34–37]. The approach is different for high pressure and low/medium pressure pipelines due to differences in their function and post-earthquake desired performance. The limitation of the ESM is that it can only be used for performance assessment of pipelines under longitudinal or lateral PGDs, but not under their combined effect. In many cases, the direction of the PGD is a combination of longitudinal and lateral PGDs relative to the pipeline where the ESM may underestimate the results. The most reliable approach for performance assessment of pipelines in liquefaction is finite element (FE) modelling, which can take the combined effect of longitudinal and lateral PGDs into consideration. FE modelling is mostly used for the performance assessment of pipelines with high importance or in cases where significant non-linear deformations is expected.

1.4. Paper outline

In this paper, the seismic performance of the Greater Tehran Area (GTA) buried gas distribution pipelines is evaluated under liquefaction. In this regard, first the performance assessment inputs, namely seismic hazard, soil type, liquefaction potential and gas pipeline network in the GTA are discussed. Afterwards, the performance of pipelines in liquefaction is assessed in two phases: (1) Extensive finite element (FE) modelling and analyses of the GTA gas distribution pipelines and evaluation of their performance in liquefaction, and (2) Validation of the methodology for developing the numerical models, which consists of an experimental program as well as the development of numerical models. FE models are developed for pipelines with various sizes, materials, end conditions, bends, and soil conditions, reflecting the variety of pipes within the GTA gas distribution network. The predicted performance of the GTA pipelines network is presented. Rehabilitation strategies are discussed for improving the performance of the system during seismic events. Countermeasures are recommended to mitigate the extent of casualties, caused by structural damage to pipelines, following major earthquakes.

The paper reports a comprehensive research study from early stages to the end, which can be used as a framework for assessment of pipeline networks under natural hazards, specifically seismically-induced liquefaction in large metropolitan areas. The FE results which are verified using the experiments can be used for fragility assessment of buried pipelines in liquefaction, while the details of the experiments are presented to be used as benchmarks for future assessments. The methodology and the framework presented in this paper can be adopted to form the basis for seismic performance assessment of any lifelines in large urban areas. A better understanding of the performance of lifeline networks and structures leads to more effective hazard mitigation techniques; ensuring a more resilient infrastructure.

2. Performance assessment inputs

2.1. Seismic hazard in GTA

Fig. 1 illustrates the major active faults in the GTA. The seismicity of the GTA has previously been assessed using different methodologies including a deterministic seismic hazard analysis (DSHA) and a probabilistic seismic hazard analysis (PSHA) [38]. For new design applications, the PSHA provides a sound approach for hazard determination and forms the basis for most design standards. However, for risk assessment of high importance structural systems, the DSHA, which provides a scenario-based hazard prediction, is recommended [39]. Therefore, in order to provide a background on the seismicity of the

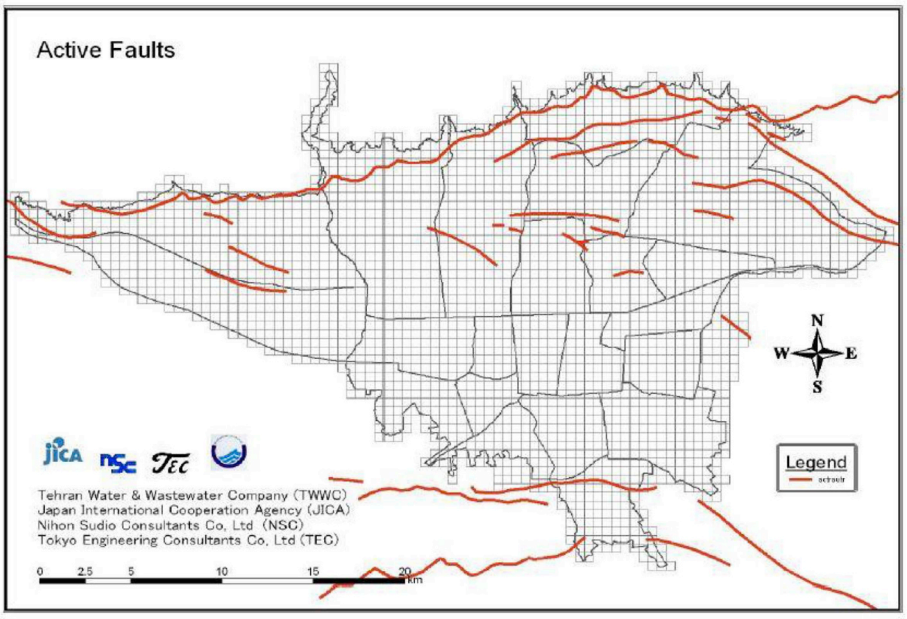

Fig. 1. Greater Tehran area major active faults (from JICA 2000 [41]).

region, the seismicity of the GTA is reported using a DSHA, based on a 10% probability of exceedance in 50 years, at each source. Such approach, although conservative, can be justified given the vulnerability of the gas distribution lifelines, the importance of their uninterrupted operation, as well as the uncertainties associated with the PSHA. Alternative methods for evaluating the seismicity of the region could be a Monte-Carlo simulation or a DSHA with a 2% probability of exceedance in 50 years.

In previous studies on the seismicity of the GTA [38,40], different seismic scenarios were considered for the region including historic and prehistoric earthquakes as well as the scenario-based earthquake for Tehran major faults. Specifically, the ground shaking associated with four different scenarios were determined. The scenarios were based on three major active faults along with a floating fault model to account for the hidden faults under the alluvial layers. The three major active strike-slip faults in the GTA are Mosha, North Tehran, and Ray faults [40]. Table 1 summarizes the faults' information and the predicted peak ground acceleration (PGA). It must be noted that the width of the fault refers to the geometric distance between the beginning and the end of the fault, in the vertical plane.

Based on the above information, using the procedure of synthesising earthquake waves and the empirical Green function method [42,43], maps in Fig. 2 were developed for the PGA distribution over the GTA corresponding to each seismic scenario. In this approach, the GTA is divided into 1 km by 1 km blocks. Next, in each block, the PGA values under each selected scenario is found, which is indicated in Fig. 2. Therefore, each block is treated as a unique site, with a unique distance to the source.

Table 1
Selected major faults in the GTA and the predicted ground motion scenarios.

Faults	Mosha	North Tehran	Ray	Floating Model[a]
Length (km)	68.0	58.0	26.0	13.0
Width (km)	30.0	27.0	16.0	10.0
Depth (km)	0.0	0.0	5.0	5.0
Magnitude (M_w)	7.2	7.2	6.7	6.4
PGA_{max} (g)	0.3	0.4	0.6	0.6

[a] Note: The length of the floating model is taken as half of the Ray fault model.

2.2. Liquefaction potential in GTA

Several studies have evaluated the liquefaction potential in the GTA. Some of such studies are presented in this Section.

The first studies were carried out in 1999 and 2000 by Japan International Cooperation Agency (JICA), as part of the microzonation of the GTA [41]. The studies focused on areas in the Southeast of Tehran, that have ground water levels less than 10 m. Hence, information from boreholes in these areas were used for the study. The selected earthquake scenario was the one associated with the Ray fault model, which has the largest PGA distribution in the area of interest. The results of this study indicated a "very low" and "relatively low" liquefaction potential for most areas in this region. This is attributed to the fact that a hard cohesive clay soil covers almost the entire area. Only in one borehole, the potential is evaluated as "relatively high". However, the liquefied soil is limited to a notably localized area and is not distributed in the region [41]. The liquefaction potential obtained from this study is shown in Fig. 3.

In the study by JICA [41], the ground settlement was assumed to be 5% of the thickness of the liquefied soil. The settlement values due to liquefaction were evaluated by the Osaka Gas company for the GTA and are shown in Fig. 4 (a). As can be observed in Fig. 4 (b), the effects of lateral spreading, which was calculated using flow potential on the slope of the area, were very low (no more than 1.5 mm) for the assessment purposes in the GTA. However, settlements are to be considered in seismic assessment.

Several research groups from the International Institute of Earthquake Engineering and Seismology (IIEES) have also evaluated the liquefaction potential in Tehran. In the first study in 1993, Hosseini and Kari [44] assessed the liquefaction potential in Southern Tehran in a medium scale evaluation. In 1998, the southwest of Tehran was studied using a PGA of 0.35 g [45], which showed a very low liquefaction potential. A joint study was carried out by the IIEES and the laboratory of Ministry of Roads and Transportation in 1999 [46] in which data from 41 boreholes in Southeast of Tehran was used. PGA distribution ranged from 0.2 g to 0.4 g, locating areas with relatively high liquefaction potential for 0.3 g–0.4 g PGAs [46]. In 2002, a large-scale study was carried out in the southeast region of Tehran [47]. The study considered site characteristics and a probabilistic seismic hazard analysis was carried out. In this study, the area in the southeast of Tehran,

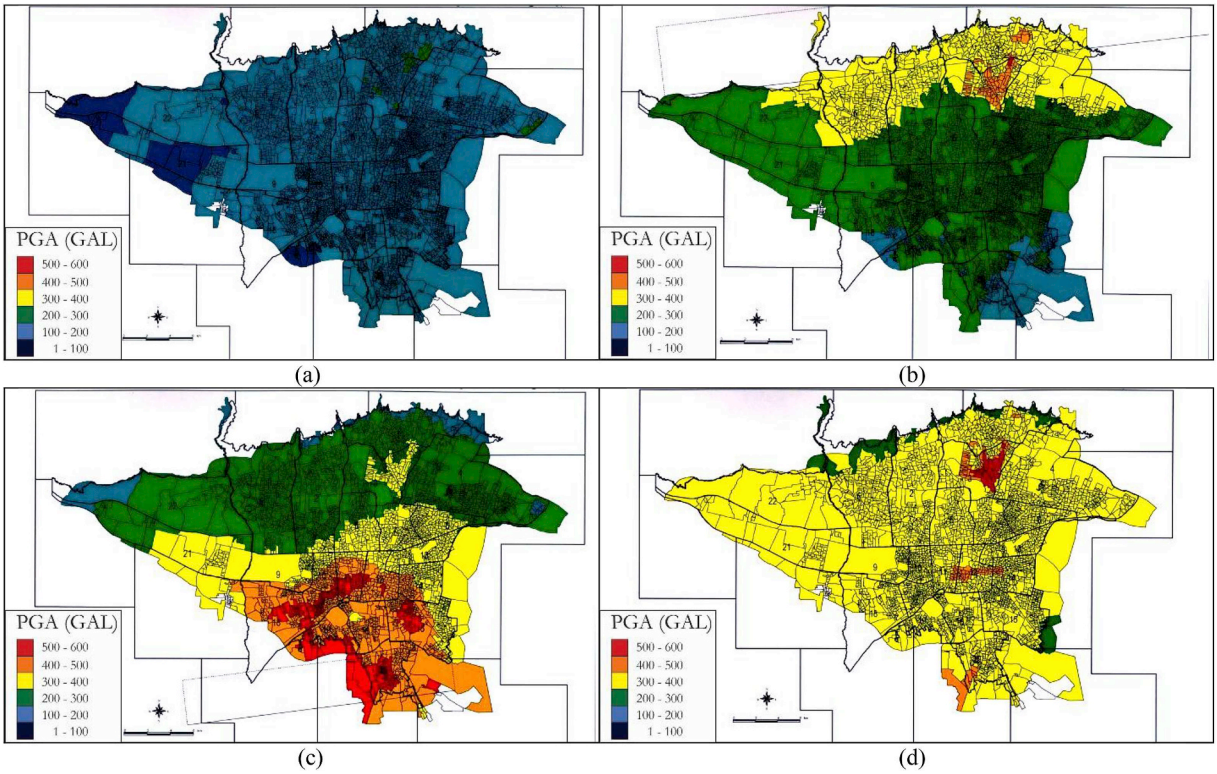

Fig. 2. PGA Distribution in the GTA Associated with each Fault-Specific Earthquake Scenario – (a) Mosha, (b) North Tehran, (c) Ray, (d) Floating Model.

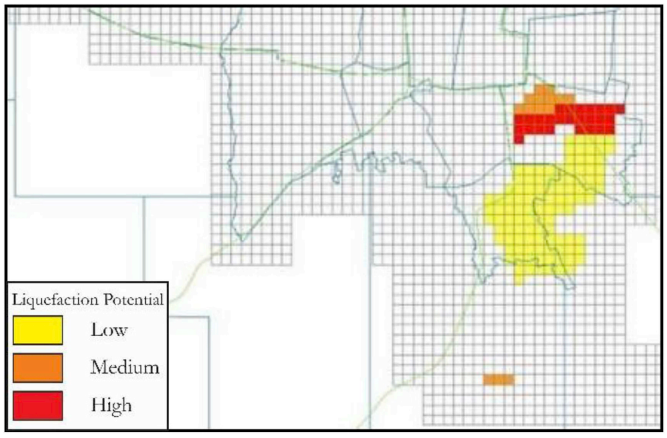

Fig. 3. Distribution of the liquefaction potential index, P_L, in the GTA.

as shown in Fig. 5(a) was divided into 1 km by 1 km blocks. Each block was assigned PGAs associated with the 10% in 50 years earthquake. The liquefaction potential for the area of interest was evaluated. Fig. 5(b) and (c) show the PGA and liquefaction potential, respectively, for the selected area in each block. Further details of this study are provided by Askari and Kasaei [47]. According to these studies, certain parts in the southeast region of the GTA have a relatively high liquefaction potential. However, most areas show a low and relatively low liquefaction potential.

Based on the findings of studies reviewed above, in the present study, the performance of gas distribution pipelines in liquefaction is evaluated only in the southeast region of Tehran, as other areas are not susceptible to liquefaction. The selected area is shown in Fig. 6 (a) and includes all regions prone to liquefaction as per previous studies [41–47]. The network of gas distribution pipelines with 250 psi and 60 psi pressures, in the selected area, are shown in Fig. 6 (b) and (c), respectively.

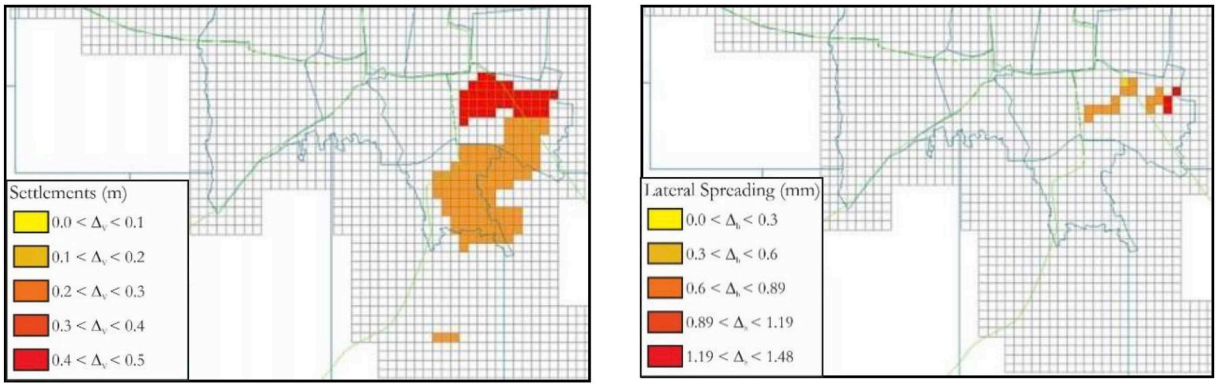

Fig. 4. Liquefaction potential in southeast of Tehran, (a) Settlements, and (b) Lateral spreading (from JICA 2000 [41]).

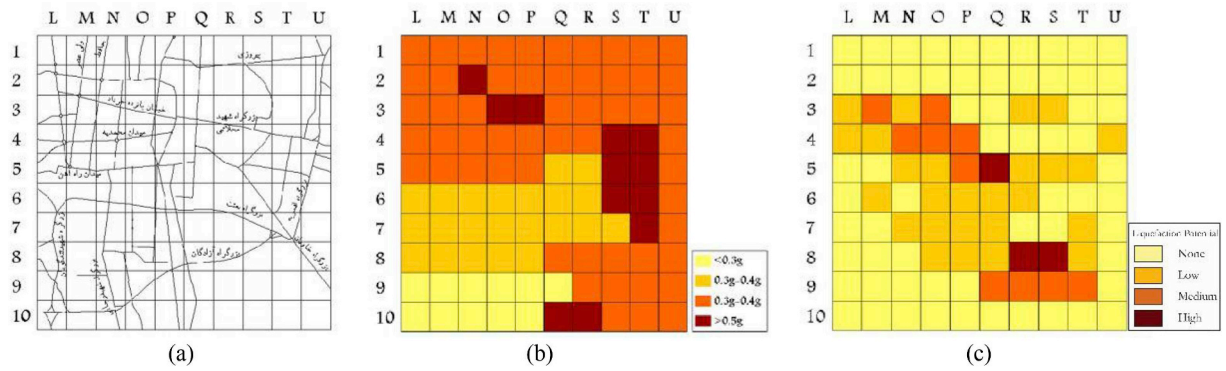

Fig. 5. (a) Discretization of the Southeast Region of Tehran for Liquefaction Potential Assessment, (b) Distribution of PGA values, and (b) Distribution of Liquefaction Potential in terms of Calculated P_L Values [47].

2.3. Soil type

As part of the study, the soil distribution maps of the GTA are gathered and the properties of the dominant soil types in the selected area for study are reviewed. Based on GTA soil distribution maps, the surrounding soil for the pipelines is formed by one of the three dominant soil types in the GTA. The soil types include dense sand (DS) with internal friction angle (ϕ) of 35°, loose sand (LS) with ϕ of 25°, and soft clay (SC) with cohesion (C) of 16.8 kPa.

2.4. Tehran gas pipeline network

Tehran gas distribution and transmission pipes form a large network

Table 2
Specifications for the Pipelines within the GTA pipeline network.

Network	Main Transmission Network	Local Distribution Network
Internal pressure	250 psi	60, 100 psi
Pipe Material	Steel: API 5L-Gr. B Steel: API 5L-X 42	Steel: API 5L-Gr. B PE: HDPE 80, 100
Pipe Diameters	2–48 inches	Steel: 2–12 inches PE: 63–160 mm
Thickness	0.068 in – 0.375 in	0.068 in – 0.375 in
Burial Depth	1–1.20 m	1–1.20 m
Coating	Tar or 3 layered PE	Tar or 3 layered PE

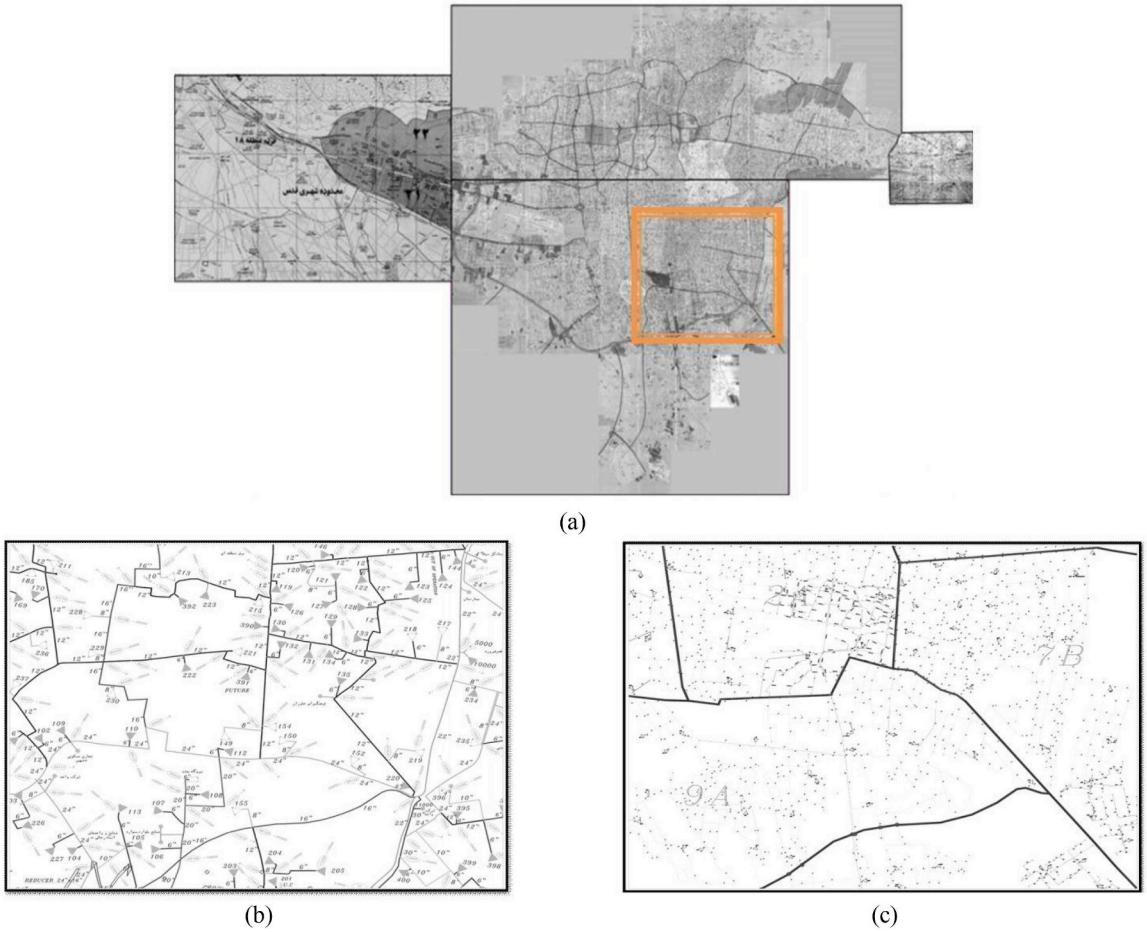

Fig. 6. (a) Selected area for performance assessment in liquefaction, (b) Network of high pressure gas pipelines, and (c) Network of medium pressure gas pipelines.

of buried pipelines. The pipeline network in Tehran consists of steel and PE pipes. The pipes' specifications, including material, size, dimensions, internal pressure, burial depth, and coating, are gathered based on available construction manuals, standards, as-built drawings, and field investigations as required. Table 2 shows the pipelines specifications for the gas distribution network in the GTA, and specifically for the selected area for study.

3. Numerical study

3.1. Equivalent static method

The Equivalent Static Method (ESM) for liquefaction performance assessment is adopted by many seismic design guidelines [34–37] and can be used in seismic design and analysis of pipelines. In this section, the method is briefly outlined. The approach is different for high pressure and low/medium pressure pipelines due to differences in their function and post-earthquake desired performance.

3.1.1. ESM for high-pressure pipelines

In its document, the Japanese Gas Association (2001) [34], provides equations for determining the distortion angle of high pressure buried pipelines subjected to liquefaction. High pressure pipelines are classified as pipes that experience internal pressures higher than 1 MPa. Different equations are provided for straight, curved, and T-portions of the pipes. The curve and bending of pipelines are defined in the plane, which can be characterized by the direction of the pipe and the direction of the settlement. In other words, it is the vertical bending and curve of the pipes that distinguishes the equations, and for horizontal bends and curves along the pipes, the equation provided for straight pipes can be used. Equation (3) provides the bending angle imposed on straight pipes due to ground movement during liquefaction [34]. Similar equations are provided for determining the bending angle in sloped areas, coastal regions, etc.

$$\omega_s = \frac{180}{\pi}\cdot 127\cdot D_i\cdot\sqrt{\frac{P_1\cdot\gamma_\delta\cdot\delta_h}{EI}} \quad \text{for } P_1 = D_i\cdot\gamma_k\cdot\sigma_c \tag{3}$$

where ω_s is the bending angle imposed on the straight pipe in degrees, D_i is the pipe diameter in meters, parameters γ_δ and γ_k are partial safety coefficients. δ_h is the soil displacement in centimeters, EI is the bending stiffness of the pipe in $N.cm^2$, and σ_c is the yielding stress of the soil in the direction of loading.

The bending capacity of straight pipelines in liquefaction is given by Equation (4) [34].

$$\omega_{sc} = \left\{0.44\frac{t_s}{D_i}\left(8k - \frac{2k^2}{3}\right) + \frac{3.44}{\sqrt{\frac{2D_i}{t_s}}}\left(1 + \frac{\varepsilon_f}{2}\right)\right\}\cdot\frac{180}{\pi} \tag{4}$$

where t_s is the pipe thickness, k is a coefficient which can be taken as 3.2, and ε_f is the ultimate strain of the pipe, suggested to be taken as 0.35.

3.1.2. ESM for medium and low-pressure pipelines

Medium pressure pipelines experience an internal pressure between 0.1 MPa to 1.0 MPa. Low pressure pipelines experience an internal pressure less than 0.1 MPa. For design and analysis of medium to low pressure pipelines, the Japan Gas Association (2003) [36] provides equations for determining the displacement capacity of pipes in liquefaction. Equations (5) and (6) provide the vertical displacement capacity for free ended pipes and clamped pipes, respectively.

$$\Delta v = \frac{2\sqrt{2}\,e^{\frac{\pi}{4}}}{D_i}\sqrt{\frac{4EI}{k_s D_i}}\,\varepsilon_0 \text{ (cm) for free ended pipes} \tag{5}$$

$$\Delta v = \frac{1}{D_i}\sqrt{\frac{4EI}{k_s D_i}}\,\varepsilon_0 \text{ (cm) for clamped pipes} \tag{6}$$

where Δv is the vertical displacement capacity of the pipe, D_i is the pipe diameter in meters, EI is the bending stiffness of the pipe in $N.cm^2$, k_s is the soil stiffness coefficient, and ε_0 is the critical strain of pipe material, which can be assumed as 0.03 for steel and PE pipes. Similar expressions are provided for determining the axial displacement capacity of steel and PE pipes with different support conditions.

In design applications, the liquefaction settlement demands are mostly assumed as amplitudes of 5 cm in each direction [36]. Hence, in design applications, the pipe performance in liquefaction can be assessed by means of comparing the vertical displacement capacity of the pipe, provided by Equations (5) and (6), with the appropriate demand based on the desired performance [36]. In the case of risk analysis, the displacement demand must be obtained according to the selected hazard level.

3.1.3. Results

Since the high-pressure pipes do not feature any vertical curves or bending, all pipelines in the area could be assumed to deform like straight pipes and the effects of curves and elbows can be neglected in the analysis. Hence, Equations (3) and (4) are used for determining the bending demand and capacity, respectively, for gas distribution pipelines in liquefaction. The partial safety coefficients, γ_δ and γ_k, are taken as 1.0 and 1.1, respectively. The ultimate strain of pipes, ε_f, is taken as 0.35. The bending demands and capacities are determined for high pressure pipelines with different size and materials, reflecting different pipe specifications within the GTA pipeline database. The results of the ESM for high pressure pipelines are presented in Table 3. As can be observed, the bending capacity of Tehran high pressure pipelines in the southeast region of Tehran is greater than the induced bending demand with a large margin of safety.

For medium and low pressure pipelines the vertical displacement capacity is determined using Equations (5) and (6). The critical strain of pipes, ε_0, is assumed as 0.03 for both steel and PE pipes. The displacement demands are selected as per the findings of previous studies by JICA and Osaka Gas Company, and are therefore, taken as 300 mm and 500 mm for the selected area under consideration. Using the ESM method, the vertical displacement capacity and demand is compared for different medium and low-pressure pipes within GTA pipe specification database. The results of the ESM for the medium pressure pipelines in the GTA are presented in Table 4. As can be observed in Table 4, some of the pipes do not have adequate capacity for the induced demand, as per the ESM.

Table 3
Results of the equivalent static method for performance assessment of high pressure pipelines in liquefaction.

Case	D_i	δ_h (mm)	Material	ω_s	ω_{sc}
1	6″	300	Steel-GrB	1.35	57.39
2	8″	300	Steel-GrB	1.18	51.99
3	10″	300	Steel-GrB	1.07	48.66
4	12″	300	Steel-X42	1.04	43.66
5	16″	300	Steel-X42	0.96	36.10
6	22″	300	Steel-X42	0.90	29.39
7	24″	300	Steel-X42	0.88	27.81
8	30″	300	Steel-X42	0.84	24.18
9	6″	500	Steel-GrB	1.74	57.39
10	8″	500	Steel-GrB	1.52	51.99
11	10″	500	Steel-GrB	1.38	48.66
12	12″	500	Steel-X42	1.34	43.66
13	16″	500	Steel-X42	1.24	36.10
14	22″	500	Steel-X42	1.16	29.39
15	24″	500	Steel-X42	1.13	27.91
16	30″	500	Steel-X42	1.08	24.18

Table 4
Results of the equivalent static method for performance assessment of medium pressure pipelines in liquefaction.

Case	D_i	Material	δ_h (cm)	ΔV (cm)	ΔV (cm) (Clamped)
1	6″	Steel-GrB	30	73.05	**11.78**
2	8″	Steel-GrB	30	96.31	**15.52**
3	10″	Steel-GrB	30	116.38	**18.76**
4	12″	Steel-GrB	30	135.53	**21.85**
13	16″	PE100	30	**5.83**	**0.94**
14	22″	PE100	30	**7.94**	**1.28**
15	24″	PE100	30	**10.58**	**1.71**
16	30″	Steel-GrB	50	73.05	**11.78**
17	6″	Steel-GrB	50	96.31	**15.52**
18	8″	Steel-GrB	50	116.38	**18.76**
19	10″	Steel-GrB	50	135.53	**21.85**
28	12″	PE100	50	**5.83**	**0.94**
29	16″	PE100	50	**7.94**	**1.28**
30	22″	PE100	50	**10.58**	**1.71**

3.2. Finite element analysis

Finite element analyses are carried out on the pipes. The pipes are modelled using beam elements with internal pressure (pipe elements). Different analytical models are constructed to reflect various pipelines, with different specifications, within the selected area. Typical stress-strain responses were used for steel and PE pipes, in the analytical models. The material models used in the numerical models are presented in Fig. 7. Steel yield and ultimate strains are taken as 0.5% and 5.0%, respectively. Elastic modulus is taken as 2.06×10^6 N/mm^2. The stress values for steel materials are provided in Table 5.

For the PE material, the ultimate strain is assumed as 8% which is a conservative assumption as this corresponds to the beginning of yielding. The selected material model for the PE pipes was based on the study by Pezeshki et al. [48].

Based on the GTA soil distribution maps and the properties of the dominant soil types, three different soil types, as described in Section 3.4, are used in the study to represent the surrounding soil for the pipelines in the analytical models. The surrounding soils are modelled as three-dimensional Winkler vertical and axial nonlinear springs using the expressions provided by the American Lifeline Alliances (ALA) [37]. The equations for soil springs and their calculated values are reported in the following section. A schematic illustration of this approach is shown in Fig. 8. In Fig. 8, t_u is the maximum soil axial resistance per unit length of the pipe, p_u is the maximum soil lateral horizontal resistance per unit length of the pipe, Q_u is the maximum uplift resistance of the soil, and Q_d is the maximum bearing resistance of the soil. These values can be determined as per the ALA provisions. The displacement values X_u, Y_p, Z_{qd}, and Z_{qu} are also determined based on the ALA provision, as reported below.

$$t_u = \pi D c\alpha + \pi D H\gamma\left(\frac{1+K_o}{2}\right)\tan\delta' \quad [7]$$

where D is the pipe diameter, c is cohesion, H is the distance between the pipe centerline and the ground surface, γ is the soil specific weight, α is the cohesion factor calculated based on c, δ is the friction angle between the soil and the pipe calculated as $f \times \phi$, where f is the friction constant based on the pipe coating, and ϕ is the soil friction angle. The value of K_o in Equation (7), can be found as (1-sin ϕ).

The value of X_u is recommended to be 3 mm, for dense sand, 5 mm for loose sand, 8 mm, for hard clay, and 10 mm, for soft clay [37].

$$p_u = N_{ch} cD + N_{ch}\gamma HD \quad [8]$$

where N_{ch} is the horizontal resistance factor for clay soil, and N_{qh} is the horizontal resistance factor for sandy soil. The value of Y_p is calculated using Equation (9).

$$Y_p = 0.04\left(H + \frac{D}{2}\right) \le 0.01D \text{ to } 0.02D \quad [9]$$

$$Q_u = N_{cv} cD + N_{qv}\gamma HD \quad [10]$$

where N_{cv} is the vertical resistance factor for clay soil, and N_{qv} is the vertical resistance factor for sandy soil. For sandy soils, the value of Z_{qu} is recommended as *0.01H – 0.02H*, but not greater than *0.1D*, for loose to dense sandy soils. For clay, the value of Z_{qu} is recommended as *0.1H – 0.2H*, but not greater than *0.2D*, for hard to soft clay [37].

$$Q_d = N_c cD + N_q\gamma HD + N_\gamma\gamma\frac{D^2}{2} \quad [11]$$

where N_c, N_q, *and* N_γ are soil resistance factors found based on the charts or equations provided by Ref. [37]. The value of Z_{qd} is recommended as *0.1D* for sandy soils and *0.2D* for clay soils.

The calculated values for the Winkler springs, for different soil types and pipes specifications, are summarized in the following tables (see Tables 6–10).

Different lengths for the liquefied area are considered in the analyses ranging from 100 m to 2 km. Pipelines are assumed to be continuous as the code specified weld is deemed sufficient for such assumption. The effects of curves along the pipelines were tested by using elbow elements in the FE models. However, as it was predicted, their effects were negligible.

The loads that the pipes are subjected to are evaluated and considered in the analysis. The soil pressure is considered in the FE models based on the weight of the soil layer above the pipes. Further, the pipe internal pressure for high and medium pressure pipes is modelled. The liquefaction loading is considered based on the results of the study by JICA [41] and the Osaka Gas company. Generally, liquefaction-induced loads must be applied to the system in terms of loads associated with buoyancy, lateral spreading, and ground settlements. The burial depth

Table 5
Steel material yield and ultimate stress values.

Steel Material	σ_y (MPa)	σ_t (MPa)
Gr. B Steel	241.0	414.0
X42 Steel	290.0	414.0

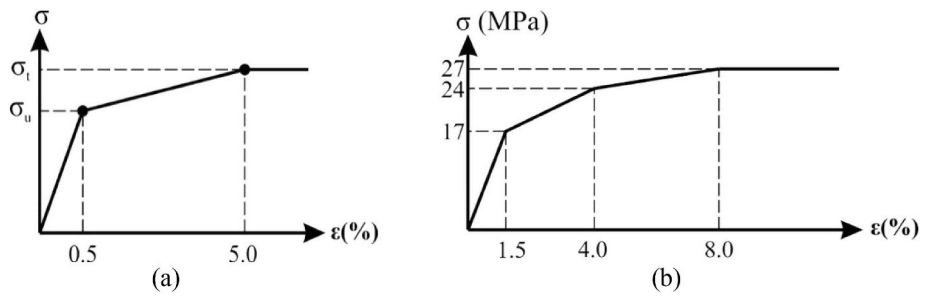

Fig. 7. Material models for (a) steel pipes, and (b) Pe pipes.

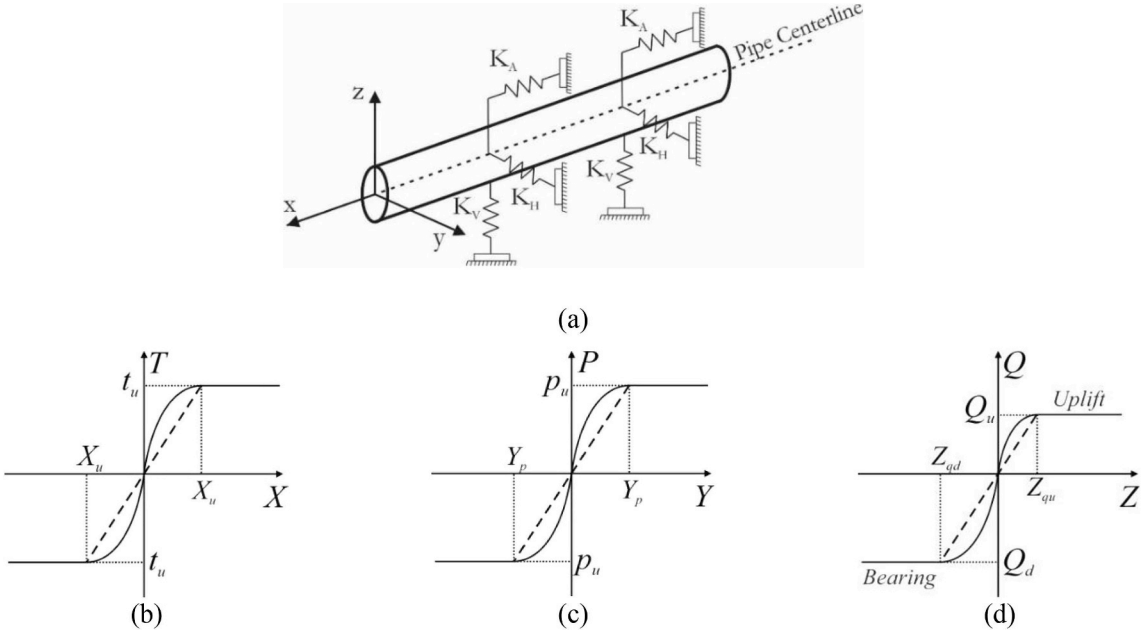

Fig. 8. (a) Schematic illustration of the 3D soil springs in the finite element models, (b) Properties of the soil springs in the axial direction, (c) Properties of the soil springs in the horizontal lateral direction, and (d) Properties of the soil springs in the lateral vertical direction.

Table 6
Soil Types and their Calculated Properties in the Finite Element Models.

Soil Type	α	c (MPa)	ϕ (Degree)	δ = f × φ	K_o	H (m)	γ (N/mm^3)
DS	1.029	0	35	28	0.43	1.2	2×10^{-5}
LS	1.029	0	25	20	0.58	1.2	2×10^{-5}
SC	1.03	0.0168	0	0	1	1.2	2×10^{-5}

Table 7
Axial spring properties for different soil/pipe types.

Pipe		DS Soil		LS Soil		SC Soil	
Material	Diameter	t_u (N/mm)	X_u (mm)	t_u (N/mm)	X_u (mm)	t_u (N/mm)	X_u (mm)
GrB	4″	2.90	3.00	2.20	5.00	5.51	10.00
GrB	6″	4.36	3.00	3.30	5.00	8.26	10.00
GrB	8″	5.81	3.00	4.40	5.00	11.01	10.00
GrB	12″	8.71	3.00	6.60	5.00	16.52	10.00
X42	12″	8.71	3.00	6.60	5.00	16.52	10.00
X42	16″	11.62	3.00	8.80	5.00	22.03	10.00
X42	22″	15.98	3.00	12.09	5.00	30.29	10.00
X42	30″	21.79	3.00	16.49	5.00	41.30	10.00
PE100	63 mm	1.80	3.00	1.36	5.00	3.41	10.00
PE100	90 mm	2.57	3.00	1.95	5.00	4.88	10.00
PE100	125 mm	3.57	3.00	2.71	5.00	6.78	10.00
PE100	160 mm	4.57	3.00	3.46	5.00	8.67	10.00

of pipelines is 1.2 m below the surface. In addition, according to the studies by JICA [41], ground water level in all locations in the GTA is 5.0 m or more from the surface. Therefore, it can be concluded that in areas with liquefaction potential, the gas distribution pipelines will not experience any buoyancy load. The level of lateral spreading is even less than pipelines' construction tolerance, and therefore, the effects of lateral spreading can be neglected in the analyses as well. The effects of ground settlements are not negligible and must be considered. As shown in Fig. 4 (a), the amount of settlements due to liquefaction is reported to be 300 mm and 500 mm in the area under consideration. These PGD demands will be applied to pipelines in the vertical direction and perpendicular to the direction of the pipelines, in the event of liquefaction occurrence. As such, they are applied in the same direction

Table 8
Lateral spring properties for different soil/pipe types.

Pipe		DS Soil		LS Soil		SC Soil	
Material	Diameter	p_u (N/mm)	Y_p (mm)	p_u (N/mm)	Y_p (mm)	p_u (N/mm)	Y_p (mm)
GrB	4″	47.86	50.03	17.94	50.03	7.46	50.03
GrB	6″	61.26	51.05	24.10	51.05	7.13	51.05
GrB	8″	73.24	52.06	29.95	52.06	6.93	52.06
GrB	12″	94.57	54.10	40.60	54.10	6.61	54.10
X42	12″	94.57	54.10	40.60	54.10	6.61	54.10
X42	16″	114.01	56.13	50.32	56.13	6.35	56.13
X42	22″	141.50	59.18	63.99	59.18	6.00	59.18
X42	30″	176.70	63.24	81.40	63.24	5.60	63.24
PE100	63 mm	34.81	49.26	12.15	49.26	7.96	49.26
PE100	90 mm	44.49	49.80	16.50	49.80	7.57	49.80
PE100	125 mm	54.25	50.50	20.79	50.50	7.28	50.50
PE100	160 mm	63.13	51.20	25.00	51.20	7.10	51.20

in the numerical models, over a limited length.

Fig. 9 shows a schematic illustration of the analytical model used in the FE analyses for performance assessment of the pipelines in liquefaction. *D* in the figure is the diameter of the pipe (see Table 9).

Performance acceptance criteria for the pipelines are selected according to the guidelines by ALA [37] and JGA [34–36] based on comparison of the strain demands with the acceptable strains. Hence, the performance of the pipes is deemed appropriate if the strain levels are below the allowable strains as per ALA [37] and JGA [34–36]. Acceptable strains are summarized in Table 11 for common failure modes in pipelines where *t* and *R* are the thickness and the radius of the pipe, respectively. It must be noted that the limit associated with the low-cycle fatigue and buckling corresponds to cases where the pipe is in compression (compressive strain), and a fatigue (cyclic) analysis has been carried out.

As previously discussed, in addition to liquefaction settlements, soil pressure and pipe internal pressures are considered in the FE analyses. Liquefaction induced settlements are inserted to the end of the soil springs and the imposed strains and stresses are obtained using a quasi-static analysis.

Table 9
Vertical spring properties in bearing for different soil/pipe types.

Pipe		DS Soil		LS Soil		SC Soil	
Material	Diameter	Q_d (N/mm)	Z_{qd} (mm)	Q_d (N/mm)	Z_{qd} (mm)	Q_d (N/mm)	Z_{qd} (mm)
GrB	4″	85.79	10.16	26.76	10.16	11.22	20.32
GrB	6″	132.14	15.24	40.71	15.24	16.84	30.48
GrB	8″	180.81	20.32	55.04	20.32	22.46	40.64
GrB	12″	285.05	30.48	84.85	30.48	33.72	60.96
X42	12″	285.05	30.48	84.85	30.48	33.72	60.96
X42	16″	398.52	40.64	116.18	40.64	45.00	81.28
X42	22″	586.04	55.88	166.04	55.88	61.94	111.76
X42	30″	868.36	76.20	237.86	76.20	84.59	152.40
PE100	63 mm	52.11	6.30	16.41	6.30	6.96	12.60
PE100	90 mm	75.53	9.00	23.62	9.00	9.94	18.00
PE100	125 mm	106.85	12.50	33.13	12.50	13.81	25.00
PE100	160 mm	139.28	16.00	42.83	16.00	17.68	32.00

Table 10
Vertical spring properties in uplift for different soil/pipe types.

Pipe		DS Soil		LS Soil		SC Soil	
Material	Diameter	Q_u (N/mm)	Z_{qu} (mm)	Q_u (N/mm)	Z_{qu} (mm)	Q_u (N/mm)	Z_{qu} (mm)
GrB	4″	22.91	12.00	16.36	24.00	17.07	240.00
GrB	6″	22.91	12.00	16.36	24.00	25.60	240.00
GrB	8″	22.91	12.00	16.36	24.00	34.14	240.00
GrB	12″	22.91	12.00	16.36	24.00	40.32	240.00
X42	12″	22.91	12.00	16.36	24.00	40.32	240.00
X42	16″	22.91	12.00	16.36	24.00	40.32	240.00
X42	22″	22.91	12.00	16.36	24.00	40.32	240.00
X42	30″	22.91	12.00	16.36	24.00	40.32	240.00
PE100	63 mm	22.91	12.00	16.36	24.00	10.58	240.00
PE100	90 mm	22.91	12.00	16.36	24.00	15.12	240.00
PE100	125 mm	22.91	12.00	16.36	24.00	21.00	240.00
PE100	160 mm	22.91	12.00	16.36	24.00	26.88	240.00

The results of the FE analyses are presented in Table 12. In Table 1, the reported strain value shows the maximum strain obtained from numerous analysis cases including straight, 45, and 90° bended pipes, cases in different liquefied area, and different boundary conditions for the pipelines. The results indicate that the high-pressure pipelines will not experience any major damage during liquefaction. Although high-pressure pipelines are expected to maintain their integrity and functionality in the event of liquefaction caused by the 10% in 50 years earthquake, they may undergo some plastic deformations. The results further indicate that small diameter PE pipes, in the southeast region of Tehran, will be subjected to liquefaction settlements beyond their capacity. Small PE pipes with diameters smaller than 125 mm may lose their functionality following a major seismic event. The results of the FE analyses are consistent with the results obtained from the equivalent static method. It was observed that internal pressures did not affect the results notably (see Table 12).

Table 11
Allowable strains in pipelines [34–37].

Pipe Material	Failure Mode	
	Low-Cycle Fatigue, Buckling	Tension
Steel	0.175 t/R	3%
PE		20%

4. Validation of the numerical model

4.1. Overview of the experimental program

The focus of the current experimental study is settlements and lateral spreading in pipeline occurring parallel with the direction of excitation. Two sets of scaled experiments are carried out. Each set contains three experiments. In the first set of experiments, the effects of ground slope on liquefaction and its effect on pipelines due to lateral spreading are investigated. In the second set of experiments, the effects of settlements due to liquefaction on buried pipelines are studied. In addition to the above-mentioned six tests, an additional pilot test is carried out in which the methodology for the construction of the soil model and instrumentation is tested. Thus, a total of seven scaled experiments are conducted. Table 13 summarizes the experiments within the experimental program.

Experiments LSP01, LSP02, and LSP03 are designed to assess the effects of ground slope and liquefaction on buried pipelines, which are aligned in the direction of lateral spreading. In addition, the effect of ground slope on the pipe demands as well as other parameters is assessed. In order to have a physical model that best resembles real-life conditions, the toe of the slope is cut with a steeper slope to allow the soil fill to move downward without much resistance. A schematic

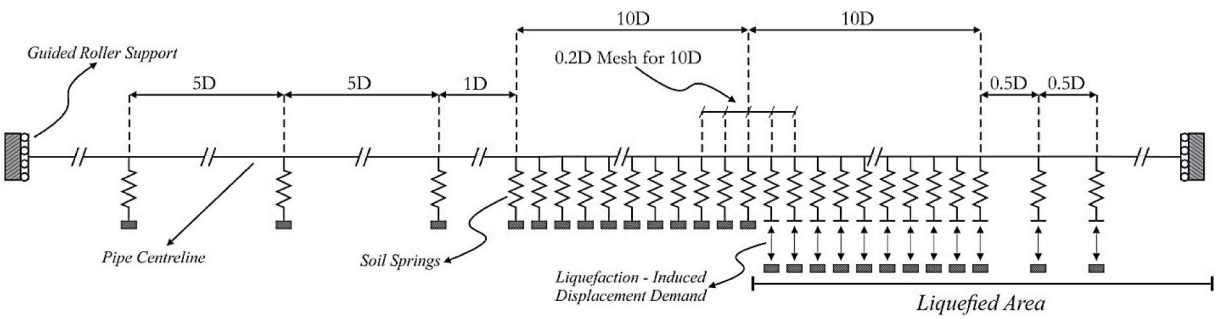

Fig. 9. Schematic illustration of the finite element model of buried pipelines.

Table 12
Results of the finite element analyses for performance assessment of pipelines in liquefaction.

Case	D	δ (mm)	Material	Internal Pressure (psi)	Max. Principal Strain	Allowable Max. Strain	Min. Principal Strain	Allowable Min. Strain
1	6″	500	Steel-GrB	60	1.54E-02	3.00E-02	−7.21E-03	−4.10E-02
2	10″	500	Steel-GrB	60	1.14E-02	3.00E-02	−5.23E-03	−3.22E-02
3	6″	500	Steel-GrB	250	1.52E-02	3.00E-02	−6.49E-03	−4.10E-02
4	10″	500	Steel-GrB	250	1.12E-02	3.00E-02	−4.55E-03	−3.22E-02
5	16″	500	Steel-X42	250	7.72E-04	3.00E-02	−5.24E-05	−2.06E-02
6	22″	500	Steel-X42	250	3.61E-04	3.00E-02	−1.03E-05	−1.50E-02
7	30″	500	Steel-X42	250	3.41E-04	3.00E-02	−1.63E-05	−1.10E-02
8	63 mm	500	PE 100	60	**4.40E+00**	2.00E-01	**−3.23E+00**	−8.10E-02
9	90 mm	500	PE 100	60	**3.44E+00**	2.00E-01	**−1.72E+00**	−8.02E-02
10	125 mm	500	PE 100	60	**2.42E+00**	2.00E-01	**−1.05E+00**	−8.03E-02
11	63 mm	300	PE 100	60	**2.00E+00**	2.00E-01	**−1.29E+00**	−8.10E-02
12	90 mm	300	PE 100	60	**8.28E-01**	2.00E-01	**−8.01E-01**	−8.02E-02

illustration of the test model, for these tests, is shown in Fig. 10 (a).

Experiments LSP04, LSP05, and LSP06 are designed to study the effects of liquefaction-induced demands on the pipelines, due to settlements. In these tests, the surface is flat and the bottom layers are liquefied to be representative of the conditions on GTA pipelines. Liquefaction of the bottom liquefied layers leads to demands in the buried pipe specimen. The varying parameters in these experiments are the relative density and the excitation acceleration amplitude. The layout of these experiments is presented in Fig. 10 (b).

For the instrumentation naming convention in tests LSP01, LSP02, and LSP03, the terms upstream, center, and downstream are used. Similarly, in tests LSP04, LSP05, and LSP06, the terms right, left and center are used to distinguish between the various instruments in the soil model.

4.2. Test setup

4.2.1. Hardware and instrumentation

The shake table used in the study is a one-dimensional shake table that is 1.8 m × 1.2 m in plan. The shake table is excited through the use of a hydraulic actuator. The hydraulic actuator has a load capacity of 25 kN and a stroke of 250 mm. For applying the seismic demands to the soil medium, the Plexiglass box containing the soil medium is fixed on the shake table. Fig. 11 shows the test setup before starting experiment LSP 02. The setup is described in detail in the following sections. The soil model, on the left, is attached to the shake table, which is excited by the hydraulic actuator on the right. The pipe specimen, while cannot be seen, is buried in the soil medium. As discussed above, it can be observed, that the toe of the soil on the left side is cut with a steeper slope. This is carried out to allow the soil to move downward more easily in order to study the effects of lateral spreading.

Physical soil models are prepared in transparent Plexiglass boxes to allow for observation of soil deformations caused by earthquake excitations. The internal dimensions of the Plexiglass boxes are 1800 mm, 450 mm, and 70 mm, for length, width, and height, respectively. At the bottom of the boxes, two valves are implemented allowing for water and Carbon Dioxide (CO_2) to enter the soil model. The bottom of the box is covered with a No. 100 screening surface. In addition to preventing the sand to enter existing valves, the screener ensures that water enters the physical model uniformly to saturate the soil model.

Five accelerometers are used to measure the applied acceleration to the soil system, in each model. The location of the accelerometers are shown in Fig. 10(a) and (b). One accelerometer is installed out of the soil model box, close to the base of the box, in order to measure the input acceleration that is applied to the system. The additional four accelerometers are installed within the soil model at distances of 100 mm, 200 mm, 300 mm, and 400 mm from the base of the box containing the soil model. All accelerometers are installed such that their positive direction is aligned with slope displacement. Normal DLT-50AS Linear Variable Differential Transformers (LVDTs) are used at the surface of the soil model to measure the ground settlements or dilation. DP-500C cable (LVDTs) are used to measure the pipe deformations. BPR-A-50KPS pore water pressure transducers (PPTs), with a pressure capacity of 50 kPa, are used to measure the pore water pressure in the soil medium. The PPTs are very small relative to the soil medium and, therefore, their effect on the soil response is very limited. The PPTs are connected and secured with a cable to assure their location does not change during the experiment.

Strain gauges are used to measure the flexural and tension demands in the pipes. Strain gauges are installed at three sections along the length of the pipe with one at the middle and two spaced at 300 mm from the center of the pipe. At each section, three strain gauges are installed as shown in Fig. 12.

4.2.2. Pipe specimen

For selecting the experimental pipe specimen diameter and thickness, the governing response mode must be considered (i.e. tensile, flexural, or local buckling). For instance, if a flexural response is the dominant response, the EI of the specimen must be primarily scaled. For axial and buckling dominant behaviours, EA and D/t must be scaled, where E is the modulus of elasticity, I is the moment of inertia of the pipe, A is the cross-sectional area of the pipe, D is the pipe diameter, and t is the pipe thickness. In the present study, the aim is to have a pipe specimen in the laboratory, representative of a real steel pipe with a

Table 13
Summary of the experimental program.

Test Name	Ground Slope	Model Accel.	Real Accel.	Loading Time	Loading Frequency	Void Ratio	Relative Density	Liquefiable Layer Thickness	Unliquefiable Layer Thickness
LSP Pilot	5.0%	0.20 g	0.30 g	5 s	3 Hz	0.84	30.0%	340 mm	100 mm
LSP 01	4.0%	0.20 g	0.30 g	5 s	3 Hz	0.87	21.5%	340 mm	100 mm
LSP 02	2.5%	0.20 g	0.30 g	5 s	3 Hz	0.89	15.6%	340 mm	100 mm
LSP 03	1.5%	0.20 g	0.30 g	5 s	3 Hz	0.90	12.6%	340 mm	100 mm
LSP 04	0.0%	0.20 g	0.30 g	5 s	3 Hz	0.90	12.6%	380 mm	100 mm
LSP 05	0.0%	0.25 g	0.38 g	5 s	3 Hz	0.75	56.7%	380 mm	100 mm
LSP 06	0.0%	0.50 g	0.77 g	7 s	5 Hz	0.75	56.7%	380 mm	100 mm

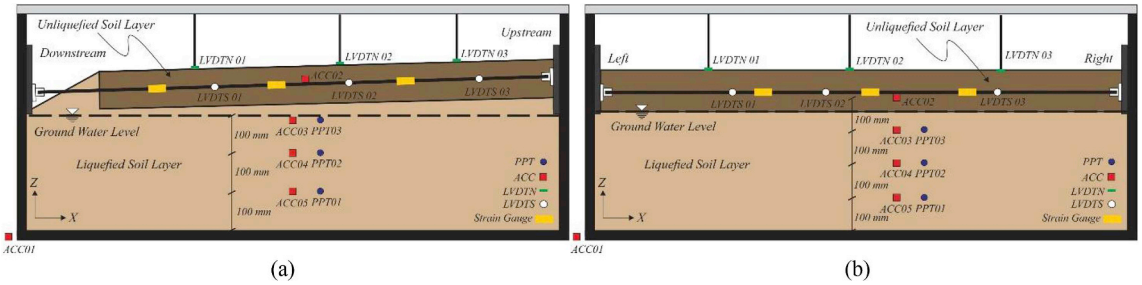

Fig. 10. Schematic illustration of soil samples (a) LSP 01–03, and (b) LSP 04–06.

dimeter of 14 in and a thickness of 17.8 mm. If EA or EI of the pipe are used to be scaled with $\lambda = 35$, diameter and the thickness of the scaled specimen will be 10 and 0.015 mm. There are no vendors that would fabricate such a pipe specimen. If the rigidity of the scaled specimen is reduced, by means of using a more flexible material such as aluminum (one-third of steel), the pipe thickness will be 0.04 mm, which still cannot be found in stock.

Since the failure mode is recognized as pipe buckling, D/t is used as the dominant scaling parameter. An Aluminum pipe specimen, with modulus equal to one-third of that of steel material, is used in the experiment to facilitate the scaling and avoid the use of excessively small physical models. Therefore, the pipe specimen is selected as an aluminum pipe with a diameter of 10 mm and a thickness of 0.5 mm. The selected aluminum pipe is scaled such that it is representative of a steel pipe with a dimeter of 14 in and a thickness of 17.8 mm, making the geometric scale factor, $\lambda = 35$.

The burial depth of the pipe in the laboratory physical model is 50 mm, which is representative of a real burial depth of 1750 mm. This burial depth is close to the GTA pipeline burial depth, which is 1200 mm. The additional burial depth makes the results of the experiment more conservative. The aluminum material elastic modulus is measured experimentally in the laboratory as 74 GPa. The support condition of the pipe specimen in the soil container in the laboratory can greatly affect the response assessment. The supports can be detailed to have a rigid, pin, or semi-rigid response. Semi-rigid supports are used for connecting the pipe to the soil container for better representation of the boundary conditions of the pipe in the liquefied area. This can be understood by considering the state of the real pipe and the scaled pipe in the laboratory during liquefaction. The length of the pipe specimen that is modelled in the laboratory is 1.61 m, which is representative of 57 m of the actual pipe in the liquefied region. However, the real pipe extends beyond the liquefied area and is indirectly affected in these regions as well. This is illustrated in Fig. 13. Modelling the supports as semi-rigid supports allows for properly capturing the response of the pipe. Also shown in Fig. 13 (b) and (c) is the pipe support detail that is

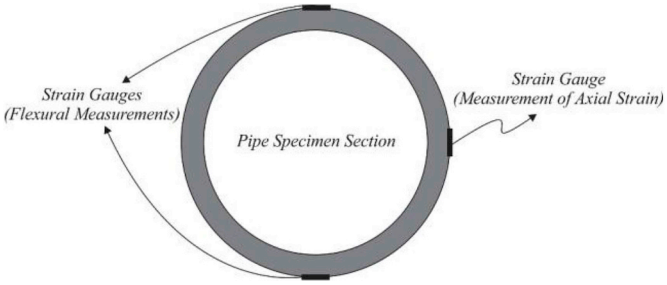

Fig. 12. Arrangement of Strain Gauges at each Instrumented Pipe Section.

used as the semi-rigid support. The support diameter is 12 mm providing 2 mm of clearance for the 10 mm pipe, which would allow pipe rotation. In addition, deformable resin material is used in the internal face of the pipe support to better resemble the real boundary conditions.

The real length of the pipe which response is replicated by the laboratory model can be determined by a few trial and errors and following simple mechanics. Three-point loads are applied to the laboratory pipe model that is constrained with the semi-rigid supports and the mid-span displacement is determined. By assuming the total length of the pipe and determining the mid-span displacements under the applied loads, using the equations for a fixed-fixed case, one can determine whether the assumed total length is reasonable or not. Thus, after a few trial and errors it was determined that the semi-rigid supports are replicating the effect of 0.45 m of pipe that extend beyond the liquefied area, as shown in Fig. 13(a). Therefore, the total length of the pipe model in the laboratory is $2 \times 0.45 + 1.61 = 2.51$ m, which is representative of a steel pipe with a length of 88 m, given $\lambda = 35$. Hence, the length of the liquefied area is 56 m and the length of the area beyond the liquefied region, which is indirectly affected by liquefaction, is 32 m.

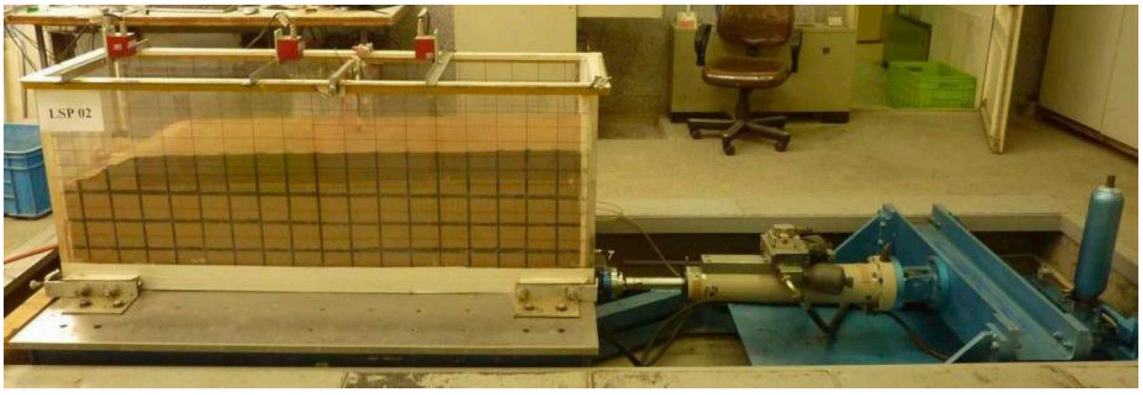

Fig. 11. Shaking table test setup showing experiment LSP 02.

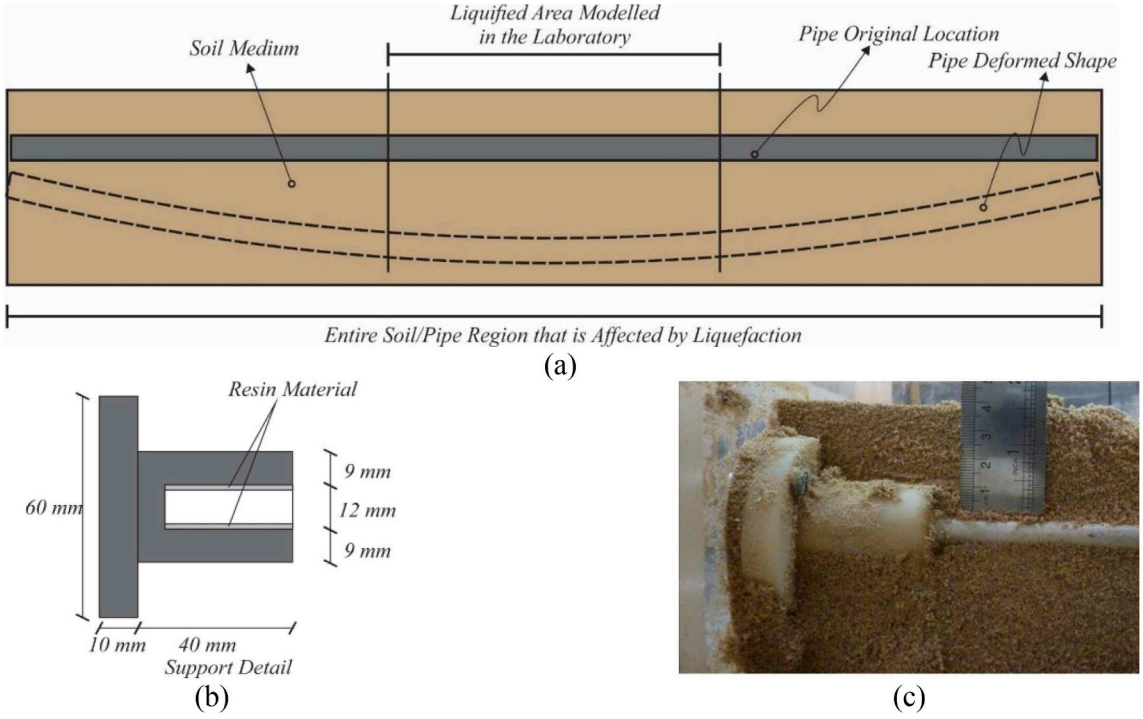

Fig. 13. (a) Illustration of the pipe liquefied region (b) illustration of the support detailing, (c) As-built pipe support.

Table 14
F161 sand properties.

Density of Particles	Maximum Void Ratio e_{max}	Minimum Void Ratio e_{min}	D_{50} (mm)	Percentage of Particles passing the No. 200 sieve (%F)	Internal Friction Angle (ϕ)	Cohesion (C)
2.658	0.943	0.603	0.3	0	37°	0

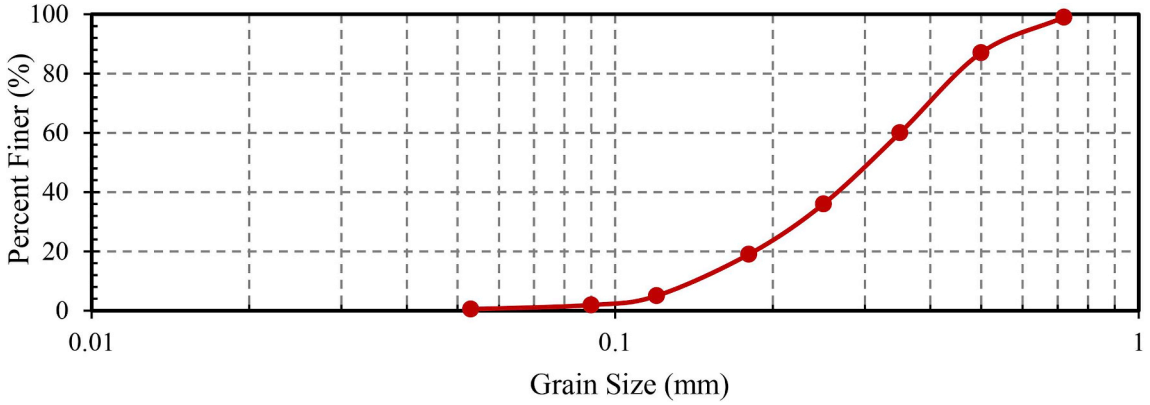

Fig. 14. Particle size distribution of the F161 sand.

4.2.3. Soil type

The selection of the soil material must be such that liquefaction, settlement, and lateral spreading occur in the experiment. For such applications, clean sands with D_{50} less than 0.5 mm have commonly been used. For instance, Toyoura sand, in Japan, and Nevada sand, in US, have been used in most scaled liquefaction experiments. Firouzkooh 161 (F161) sand, in Iran, has many similar characteristics to the above-mentioned sands and is, therefore, used in the present study. The characteristics of the F161 sand is summarized in Table 14. In addition, the particle size distribution for the F161 sand is shown in Fig. 14.

4.3. Excitation

Seed and Idriss [26,27] have shown that the effects of an earthquake can be replicated with an excitation with certain amplitude and number of cycles. On this basis, Seed and Idriss have proposed a methodology to replicate the effects of liquefaction caused by an earthquake, by applying a harmonic excitation to system. The amplitude of the excitation is to be scaled such that it produces a response that is 65% of the peak response spectrum caused by the ground motion. The number of cycles is determined based on the earthquake magnitude [49]. It has been shown that accumulated strain energies obtained from a real

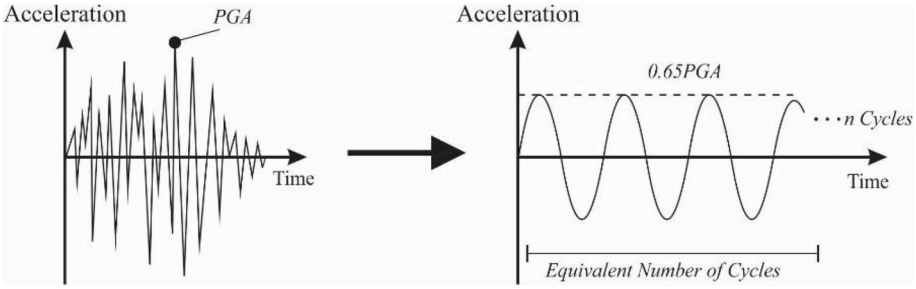

Fig. 15. Schematic illustration of the applied excitation.

earthquake excitation and from the uniform excitation method by Seed and Idriss are similar [50]. The same approach is used for determining the excitations in the experimental program. The PGA and the number of cycles are chosen to be representative of the seismological characteristics of the GTA. A schematic illustration of this is shown in Fig. 15.

4.4. Results

The soil models before and after the experiments are shown in Fig. 16, for all tests. In all experiments, it is observed that pore waters reached the soil surface upon completion of the test. This is often accompanied with sand boiling. The results are reported with more details for experiments LSP01 and LSP04. For the other tests, only results that extensively vary from the reported cases are discussed.

4.4.1. Experiments LSP 01 – LSP 03

Experiments LSP01, LSP02, and LSP03 are performed on soil models in which the ground surface and the pipe specimens were slopped. It can be observed that during liquefaction, soil middle layers have undergone lateral spreading and moved horizontally. As such, after the test the surface is effectively flat. The unliquefied layer has not undergone any lateral spreading and has only experienced vertical movement, which is caused by the slope failure in liquefaction.

The pipe bending moment and axial strain time-histories are shown in Fig. 17, for LSP 01. The bending moment and axial strain demands are maximum at upstream. It can be observed that in all cases, the bending moment tends to reach a peak value and then reduce during the response. One reason for this behavior is the fact that after slope failure the soil medium flows horizontally which reduces the pipe bending moments. In addition, due to lateral spreading, the height of soil above the pipe will decrease, which causes the bending moments to decrease, with the exception that for the downstream region the soil height above the pipe will increase due to slope failure. Therefore, the second mechanism counteracts the previous one and the bending moment at downstream will remain unchanged. It is further observed that the upstream tensile axial strain is much more significant than other locations.

The displacement time-histories for ground and the pipe specimen are shown in Fig. 18 (a). It can be observed that after initiation of ground excitations, lateral movement of the soil layer starts until reaching its maximum value. The lateral displacement remains effectively constant after that, with vibrations during the excitation. Ground settlements decrease by moving from the upstream end to the downstream. The reason for this is the lateral movement and settlement in the soil. At the downstream location, the settlement effects are counteracted by the horizontal flow of the soil due to slope failure. Therefore, at this location smaller settlements are observed. Selected response parameters are plotted in Fig. 18 (b). This is done to recognize the behavior of the system in terms of different response parameters at the beginning of the excitation, during liquefaction, and after the excitation is over. It is after liquefaction that the pipe experiences permanent axial strains. Tensile axial strains are induced on the pipe in the upstream region, where towards the center and downstream, the axial strains are effectively negligible.

In Experiment LSP02, contrary to Experiment LSP01, the bending moment in the downstream is increased. In this case, the extent of settlements is less than the increase in the soil height above the pipe, causing the pipe bending moment at this location to effectively increase. Similar to the previous case, the bending moment at center and upstream has decreased. Similar to the previous test, upon liquefaction, the pipe experiences its maximum demands and is not much affected by the following cycles. All of the observations for experiment LSP 01 hold for experiment LSP 02 as well. The only difference is that the axial strains at the center are no longer negligible and have positive values, representing tension. Further, the pipe experiences negative axial strains at the downstream end, representing compression.

In experiment LSP 03, the pipe bending moment undergoes reductions at all three locations, with the downstream bending moment increasing after its reduction. Similar to previous cases, the pipe experiences the lowest bending moment reduction at the downstream location as the height of soil above the pipe has seen the least amount of reduction. Further, the pipe experiences tension at all locations, with the upstream axial tension being much higher than the center and downstream values. All other observations in experiment LSP03 are the same as those observed in experiments LSP01 and LSP02.

It must be noted that although the pipe experiences compression at the downstream location, in one case, and tension, in the other two cases, the general trend of the axial strain is the same in all liquefaction experiments with sloped ground. In all cases, upstream axial strain is recorded as tension and is reduced by moving from upstream to downstream.

4.4.2. Experiments LSP 04 – LSP 06

The pipe bending moment and axial strain time-histories, for experiment LSP 04, are shown in Fig. 19. Ground displacements along with additional response parameters are presented in Fig. 20 (a) and (b). It can be observed that the bending moment on the right side of the pipe do not significantly and stay the same. However, on the left side, a reduction is observed. By studying the displacement time-histories, it can be observed that ground displacement on the left side is higher than the ground displacement on the right side, which is the reason for reduction in bending moment at this location. The strain time histories indicate that the pipe experiences tensile demands on the left side and at the center. The pipe residual axial strains on the right side are negligible. However, during ground shaking, the pipe experiences significant tensile strains, which must be considered in design applications. The reason is that the soil experiences lateral movements during the excitation, which are transferred to the pipe through friction between the pipe and the soil medium, leading to significant axial demands. Displacement time histories show that the pipe effectively does not experience much movement. However, soil settlements are observed.

In test LSP 05, the relative density of the soil model is increased to 50% and the input excitation is increased to 0.25 g. After applying the excitation to the soil sample, the soil did not reach a liquefied state.

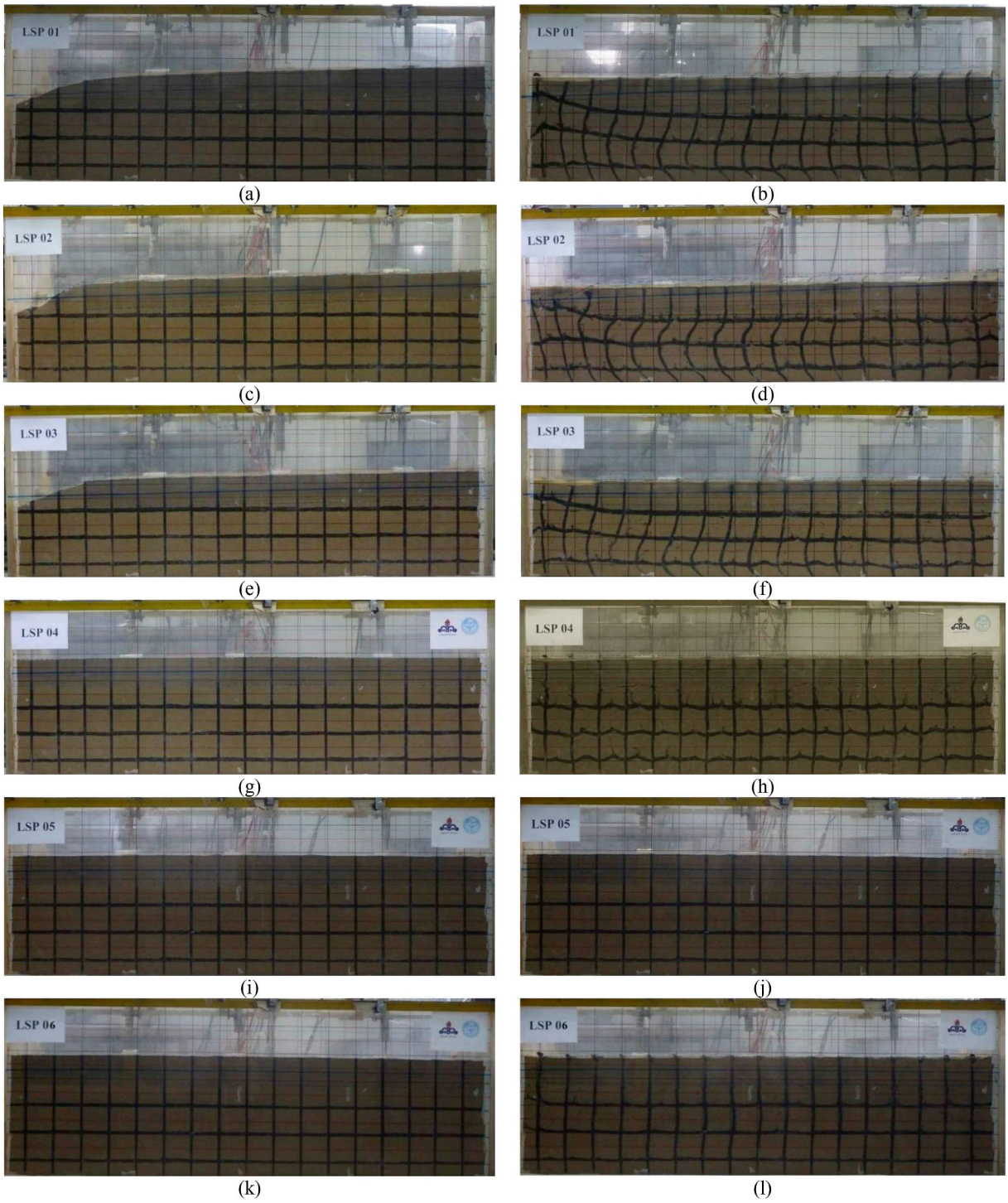

Fig. 16. Condition of the physical soil models before and after the excitations.

This can be observed by looking at the pore water pressure recordings, in Fig. 21 (a). As can be observed from Fig. 16, the condition of the soil model is not different prior to and after the test. Bending moment and axial strain demands are very limited. The pipe experiences limited flexural demands at the left side and the center, with a bending moment of roughly 200 N m. Further, a compressive axial strain of 0.01, at the left side of the pipe, is observed. These demands are very small compared to the demands in previous tests. As expected, ground and pipe displacements are effectively zero in all directions.

It can be observed that the general trend of the pore water pressure graphs is different in the case where no liquefaction has taken place. In cases with liquefaction, the pore water pressure stays constant for some time and then starts to dissipate. However, in this case, after the excitation pore water pressure decreases rapidly resembling the response of an unstable equilibrium, similar to the post-buckling response of a steel brace in compression. In addition, it is observed that the pore water pressure values at all soil layers are equal. Both of these observations occur in cases where no liquefaction has taken place.

Since the physical model in experiment LSP 05 did not reach a liquefied state, the soil model is subjected to another excitation in experiment LSP 06. A sinusoidal excitation with an acceleration amplitude of 0.5 g, a frequency of 7 Hz, and a total time of 7 s is applied to the

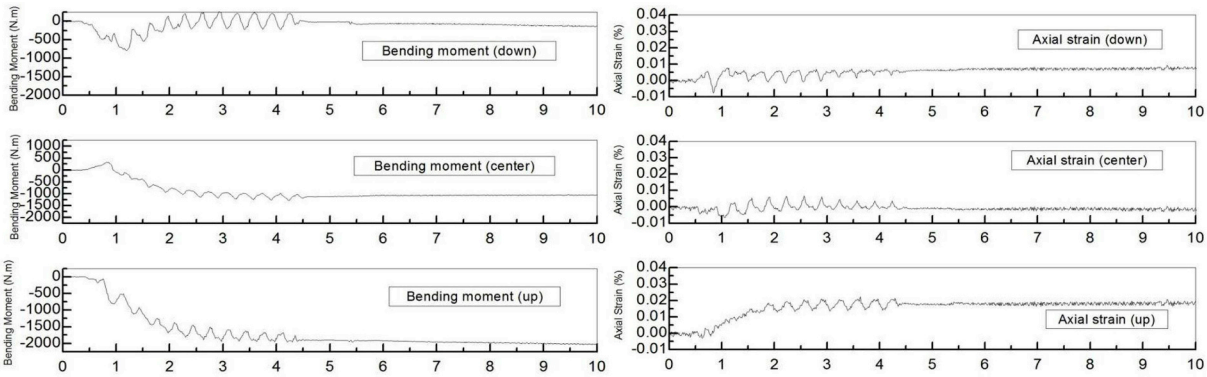

Fig. 17. Pipe bending moment and axial strain time-histories for experiment LSP 01.

soil model, making a total of 35 cycles. In this experiment, the soil reached the liquefied state. The pore water pressures for experiment LSP06 are shown in Fig. 21 (b).

4.4.3. Effects of lateral spreading on pipelines subject to liquefaction

In all three experiments, it is observed that the vertical movement of the soil layer is greater than that of the pipe specimen. This shows that in performance assessments of buried pipelines in liquefaction, applying the ground vertical displacements to the pipe will lead to results with acceptable conservatism. The same has been done in the present study for performance assessment of the GTA buried gas pipelines in liquefaction. PGDs are observed to be proportional to ground surface slope. This is expected, as higher slopes result in a greater horizontal component of the gravity load, increasing the extent of lateral spreading. The observed PGDs are summarized in Table 15 for experiments studying lateral spreading in liquefaction.

The demands on the pipe specimen are measured as axial strains caused by axial and flexural actions. The maximum absolute axial strains along the pipe section in each specimen are summarized in Table 16, along with the maximum absolute residual axial strains. It must be noted that residual strains, in this case, could exceed the maximum transient strains that were experienced in the soil layer during the excitation. The reason is that often the ground movement will continue even after the end of the excitation.

4.4.4. Effects of settlements on pipelines subject to liquefaction

As was the case in previous experiments, the ground settlements are observed to be more significant than the vertical displacements induced in the pipe specimen. As such, applying the ground displacement to the pipe specimen, as the liquefaction induced demand, will result in a performance assessment with a reasonable level of conservatism. Maximum absolute values of measured strains are reported in Table 17, for experiments LSP 04, 05, and 06.

One of the observations from Table 17 is that the residual strains

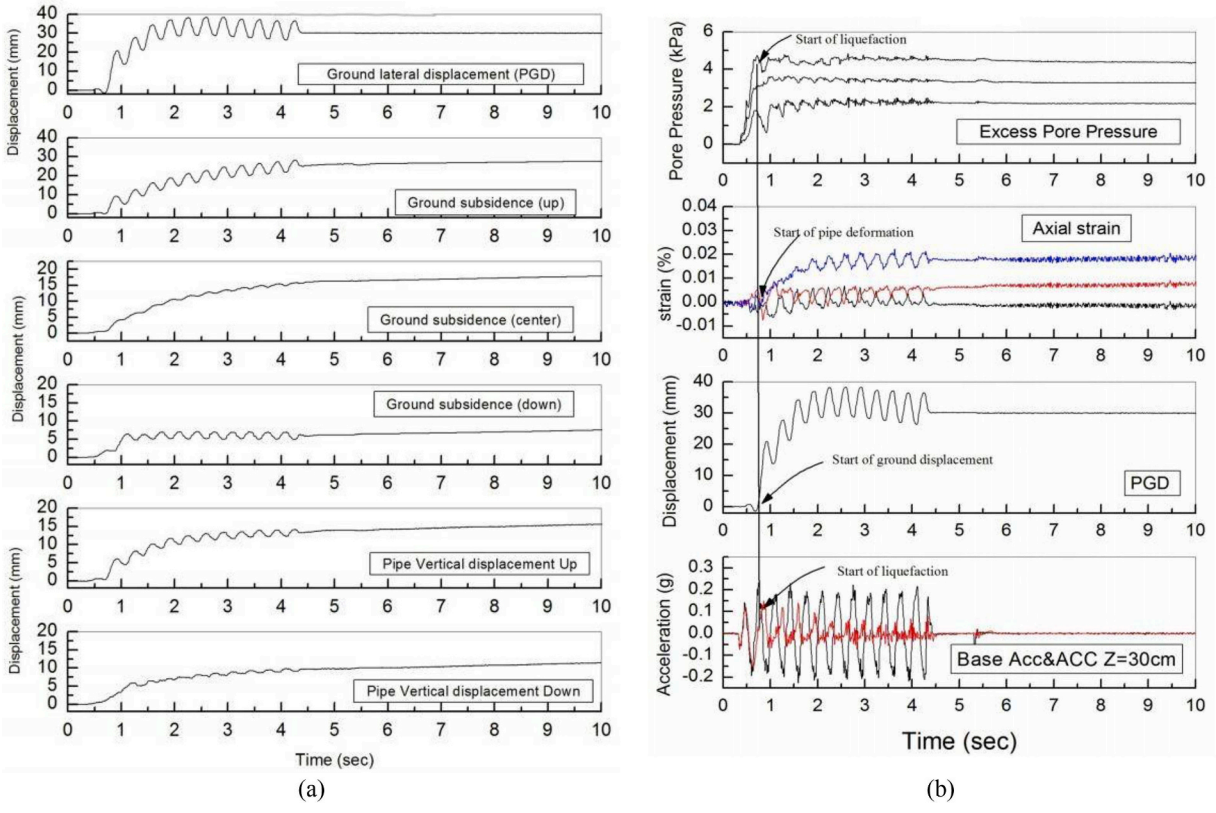

Fig. 18. Results of experiment LSP01 (a) ground displacement time histories, and (b) Selected response parameters.

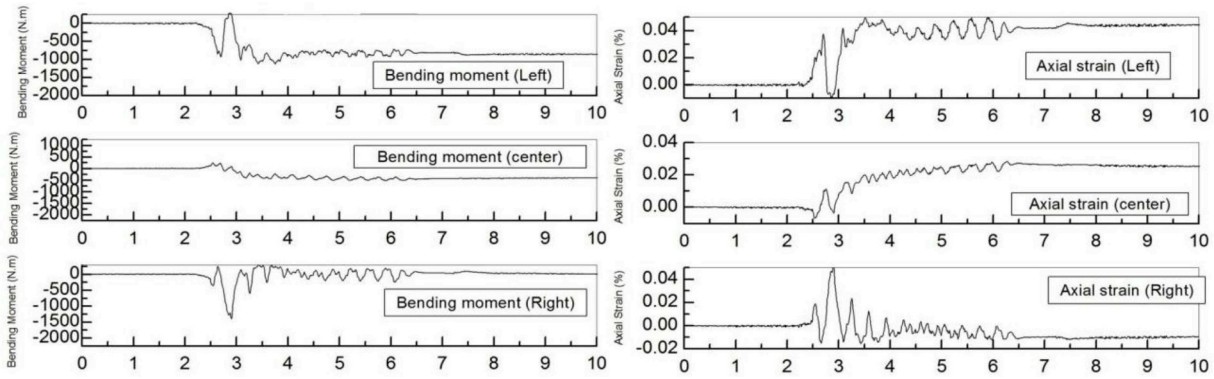

Fig. 19. Pipe bending moment and axial strain time-histories for experiment LSP 04.

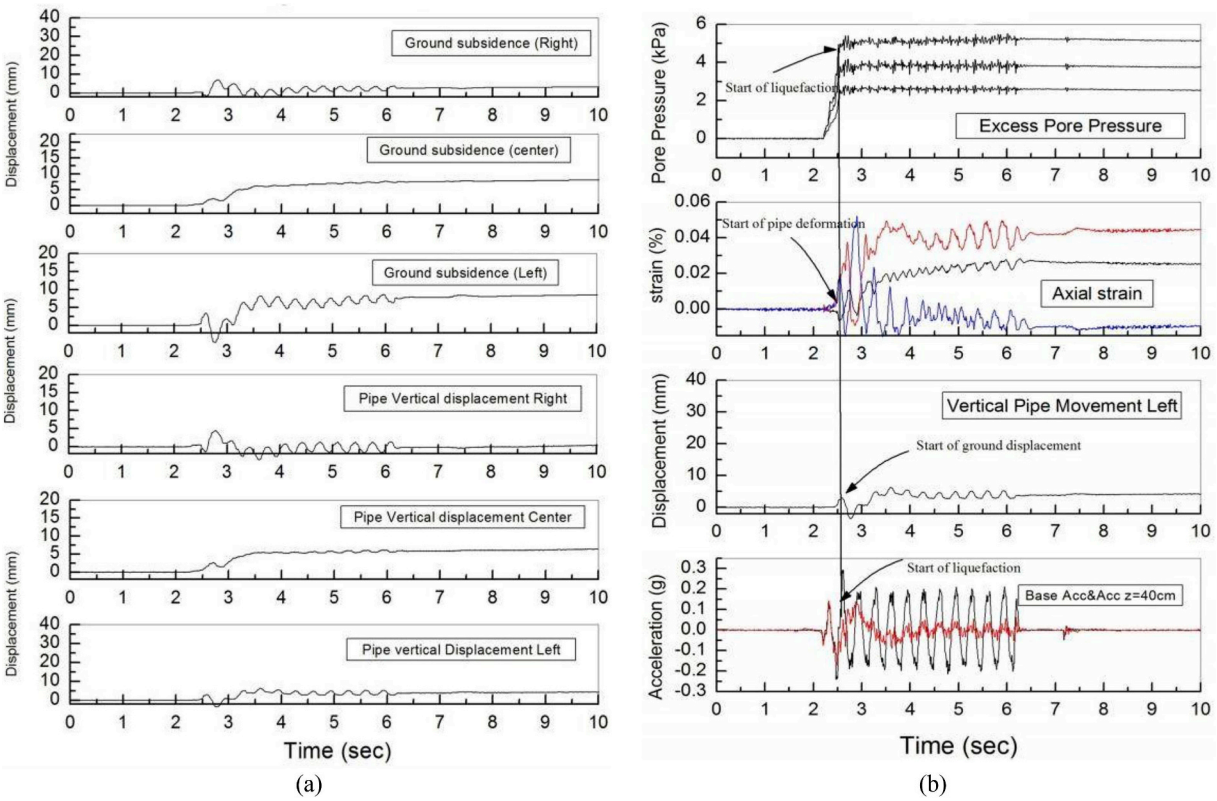

(a) (b)

Fig. 20. Results of experiment LSP04 (a) ground displacement time histories, and (b) Selected response parameters.

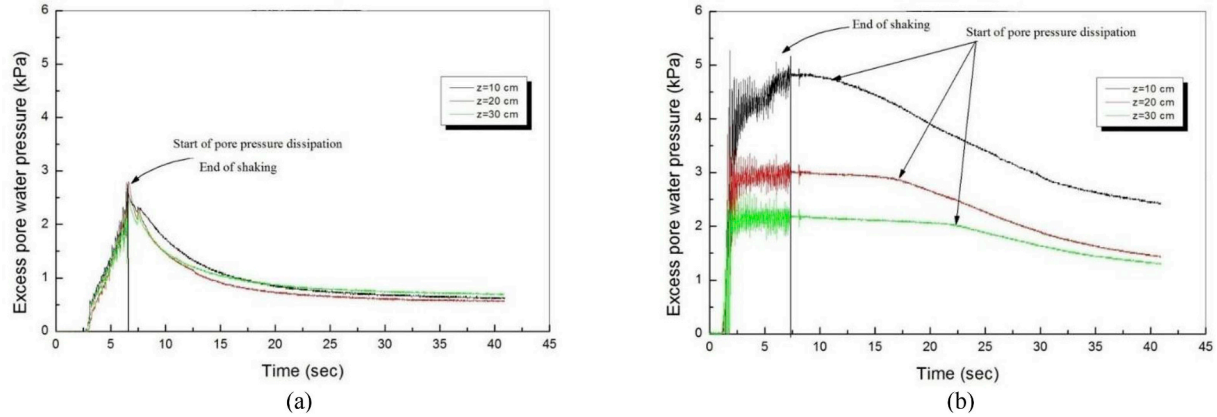

(a) (b)

Fig. 21. Pore water pressure time histories, (a) LSP 05 – No liquefaction, and (b) LSP 06 - liquefaction.

Table 15
Summary of PGDs for experiments LSP 01, LSP02, and LSP03.

Experiments	Ground Slope (%)	Laboratory Model PGD	Actual PGD
LSP 01	4	29.9 mm	1.05 m
LSP 02	2.5	21.9 mm	0.77 m
LSP 03	1.5	11.3 mm	0.40 m

are, almost in all cases, smaller than their corresponding transient values. Therefore, it can be concluded that although after liquefaction soil will continue to settle, the post-shaking settlement induced strains do reach strains that were experienced during the excitation. In other words, in liquefaction without lateral spreading, the extent of damage during ground shaking is greater than secondary damage caused by post-shaking actions. The demands on buried pipelines are dependent on the input excitation and soil properties. For instance, although the input excitation is more severe in experiment LSP06, compared to experiment LSP04, higher demands are observed in experiment LSP 04. The reason is that the soil medium in experiment LSP06 is much denser.

4.5. Baseline model validation

The tests within the experimental program are designed to be representative of the GTA gas distribution pipelines. For instance, as it is the case for the GTA gas distribution network, in the physical models, pipelines were located in the unliquefied soil layer, above the liquefiable layers. Therefore, the results of the experimental program can be used to improve and validate the assumptions in the finite element models, used in the performance assessment of the GTA buried gas pipelines. For this purpose, baseline FE models of the pipe specimen in each experiment are developed. The pipe specimen is representative of a steel pipe with a diameter of 356 mm, a thickness of 17.8 mm, buried at a depth of 1750 mm below surface. The total length of the liquefied area is 52 m, for experiments with lateral spreading, and 60 m, for experiments without lateral spreading. Since, the soil effects are modelled using nonlinear soil springs, for the finite element models, only the properties of the soil layer which contains the pipe specimen is required. In all experiments, the unliquefied soil layer containing the pipe specimen consists of Sand and Clay with its cohesion (C), friction angle (ϕ), and density (γ), specified as 25 KPa, 38°, and 18 k/m^2, respectively. Liquefaction induced demands are applied to the pipe specimen as quasi-static displacements at the end of the soil springs. Ground settlements in the experiments are summarized in Table 18.

Semi-rigid supports are used for the pipe boundary conditions. The rigidity of the supports are selected to represent the case where the pipe extends beyond the modelled liquefied region by a quarter of the length of the modelled liquefied area. Finite element models of the pipe specimen are developed for experiments LSP 04, 05, and 06. Nonlinear soil springs are used in the model to capture the soil behavior, as per the provisions of ALA [37]. A schematic illustration of the pipe FE model is shown in Fig. 22.

In the present study, experiments LSP01, 02, and 03 are representative of pipelines susceptible to lateral spreading caused by liquefaction. As discussed previously, the studies by JICA, the Osaka gas company, and research groups in the IIEES showed that the GTA is not susceptible to lateral spreading [41,44–47]. However, ground settlements are expected in the GTA, in the event of liquefaction. Therefore, finite element models of experiments LSP 04 and LSP 06 are developed and verified with experimental results. Experiment LSP05 was omitted in the FE verification study. The reason is that the soil model, in test LSP 05, did not reach a liquefied state and, therefore, results cannot be used, objectively. The results from the FE models are summarized and compared to their corresponding values in Table 19.

As can be observed, the results from the numerical models show slight deviation from the experimental results. The reason is the fact that in the numerical models, liquefaction demands are applied to the system as quasi-static displacements as oppose to dynamic excitations. In addition, in the experimental program it is observed that ground settlements are always greater than pipe displacements. Therefore, if one uses the ground displacements to obtain the demands on the pipe, the analysis will be conservative yet acceptable. This assessment is consistent with the results observed in Table 18. As can be observed, the results from the numerical models slightly overestimate the experimental results. This is an acceptable level of precision from a practical standpoint. Further, the goal of the present study is to assess the performance of a comprehensive database of buried pipeline within the GTA. For such performance assessments, use of acceptably simplified assumptions is acceptable to keep the study computationally efficient. Therefore, the predicted strain values indicate that the boundary conditions are adequately captured by the Winkler model in the FE approach and the pipe element can adequately predict the performance of the pipelines. Hence, the simplified decoupled FE model used in the numerical study, where the PGDs (settlements or lateral deformations due to liquefaction) were applied as static deformations to the pipe and spring model is validated.

4.6. Conclusions/counter measures

The performance of the GTA gas distribution pipelines is evaluated in liquefaction by means detailed FE analyses, in the southeast region of Tehran. The selected area, which has the highest liquefaction potential in the GTA, is chosen according to the findings of previous studies [41,44–47]. The FE analyses include a comprehensive database with different pipe geometries, sizes, material specifications and boundary conditions, reflecting the variety of pipes within the GTA gas distribution network. The study is also accompanied with an experimental program, which include shaking table tests on 7 scaled soil medium/pipe specimens. The test setup is designed to be representative of the geotechnical characteristics of the GTA. Results from the experimental program are used to verify the FE models used for the performance assessment of buried pipelines in the southeast of Tehran. The present study leads to the following conclusions.

1. In experiments accompanied by lateral spreading, it is observed that the liquefied soil layers had the tendency to move in the downstream direction. This will cause the surface to become effectively flat and will induce significant demands on the buried pipeline.
2. In experiments LSP05 and LSP06 the soil model density is increased, which increases the pore water pressure threshold at which liquefaction occurred in the soil model. Therefore, the

Table 16
Pipe axial strains for experiments LSP 01, LSP02, and LSP03.

Experiments	Upstream		Center		Downstream	
	Maximum Transient	Maximum Residual	Maximum Transient	Maximum Residual	Maximum Transient	Maximum Residual
LSP 01	0.181	0.199	0.110	0.087	0.067	0.035
LSP 02	0.151	0.131	0.135	0.140	0.150	0.101
LSP 03	0.139	0.146	0.111	0.114	0.176	0.117

Table 17
Pipe axial strains for experiments LSP 04, LSP05, and LSP06.

Experiments	Upstream		Center		Downstream	
	Maximum Transient	Maximum Residual	Maximum Transient	Maximum Residual	Maximum Transient	Maximum Residual
LSP 04	0.162	0.038	0.094	0.094	0.137	0.103
LSP 05	0.012	0.005	0.028	0.020	0.031	0.027
LSP 06	0.069	0.031	0.064	0.027	0.070	0.036

Table 18
Summary of ground settlements in the experiments.

Experiment	Downstream/Left Settlements (mm)		Center Settlements (mm)		Upstream/Right Settlements (mm)	
	After Shaking	At t = 40 s	After Shaking	At t = 40 s	After Shaking	At t = 40 s
LSP01	207	483	560	837	882	1193
LSP02	74	305	550	851	718	991
LSP03	368	630	413	704	438	718
LSP04	266	455	259	445	88	259
LSP05	14	35	49	63	53	53
LSP06	315	389	235	319	140	203

Table 19
Comparison of the Results from the FE Model vs the Experimental Results for Experiments LSP 04 and LSP 06.

Experiment	Right Settlement	Center Settlement	Left Settlement	Maximum Pipe Strain	
				Numerical	Physical Model
LSP04	455 mm	445 mm	259 mm	0.123	0.103
LSP06	389 mm	319 mm	203 mm	0.041	0.036

resistance of the soil medium to liquefaction is increased by higher soil density and stronger motions are required to liquefy the soil. However, even if liquefaction occurrence is prevented by compaction, seismic wave propagation within the soil medium and its interaction with the pipe specimen, leads to demands on the buried pipeline. Although these demands are generally less significant compared to liquefaction-induced demands, designers must consider wave-propagation demands in the design of buried pipelines.

3. In the event of liquefaction caused by a major seismic event, the high-pressure pipelines in the southeast of Tehran are not expected to undergo any significant damage and pipeline integrity is likely to be maintained. However, they may exhibit plastic deformations. Therefore, field inspections and forensic analyses for high-pressure pipelines are recommended following future seismic event.
4. The occurrence of plastic deformations in the pipelines in the event of an earthquake is more severe for medium pressure pipes (60ksi) in the southeast region of Tehran. Further, the performance assessment of pipelines under liquefaction illustrated that small diameter PE pipes are likely to lose their integrity un der liquefaction in the GTA. This was shown in the numerical study, using both the ESM and in the FE analyses. The results of the FE analyses can serve as a stronger basis to identify the extent of damage, as they are based on strain values.
5. The most effective counter measure to mitigate the risks in liquefaction is to remove the hazard itself. This can be done by improving the soil and by increasing the underground water levels. Soil improvements can be done with compaction of the soil layers or with injection to the soil layer.
6. It is vital that lifeline networks maintain their integrity after seismic events. This can be ensured by proper design and detailing of the pipes, use of automatic shutoff valves, and increasing the redundancy of the system by implementation of alternative additional transmission paths.
7. It is recommended that highly damaged areas in the southeast region of Tehran, which is selected in the current study, be marked for urgent post-earthquake measures to check the safety of pipelines. In addition, use of shut-off valves as a retrofitting strategy is recommended for the pipelines in this region, especially for the PE pipes.
8. Since currently there is no real-time monitoring system for the GTA gas distribution network, urgent post-earthquake action and investigations are necessary to diagnose the disruptions and stop the flow in damaged pipes. It is further advised to arrange for several emergency stations for field patrol and post-earthquake countermeasures in the highlighted areas.
9. The necessity of establishing a real-time monitoring system such as SCADA, for all types of lifeline systems in Tehran is recognized. The SCADA must be synchronized with a dense array of seismographs for real-time monitoring and immediate measures in the event of earthquakes.
10. As a long-term loss-mitigation strategy, the vulnerable medium pressure pipelines can be replaced with PE pipes. However, the most feasible short-term mitigation strategy is the implementation of the monitoring system and the use of automatic shutoff valves.

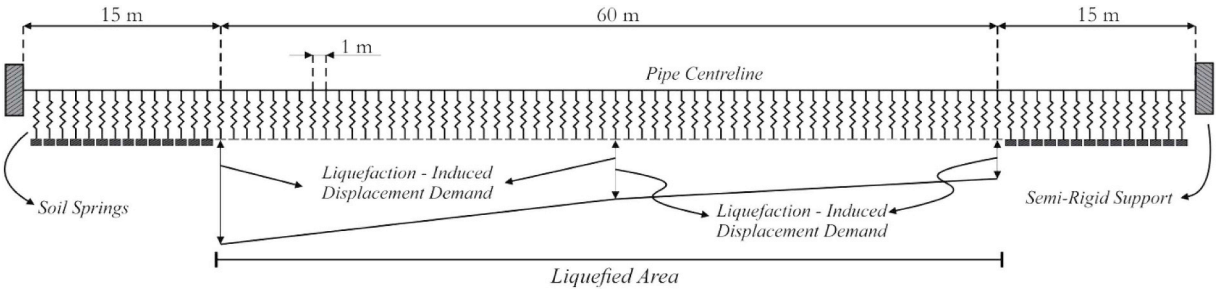

Fig. 22. Schematic Illustration of the FE Model used for Verification of the Numerical Model with Experimental Results.

Acknowledgements

This project has been funded by Tehran Province Gas Company. The authors would like to thank the organization and acknowledge their support throughout the project. Also, the authors wish to extend their thanks to Prof. Khosrow Bargi of University of Tehran for his kind support and management during the project.

Appendix A. Supplementary data

Supplementary data to this article can be found online at https://doi.org/10.1016/j.soildyn.2019.05.033.

References

[1] Liu A, Hu Y, Zhao F, Li X, Takada S, Zhao L. An equivalent-boundary method for the shell analysis of buried pipelines under fault movement (2004). Acta Seismol Sin 2004;17(Suppl 1):150https://doi.org/10.1007/s11589-004-0078-1.
[2] Shinozuka M, Takada S, Ishikawa H. Some aspects of seismic risk analysis of underground lifeline systems. J Press Vessel Technol 1978;101(Issue 1):31–43.
[3] Toki K, Takada S. Earthquake response analysis of underground tubular structure (1974). Bull Disaster Prev Res Inst 1974;24(2):107–25.
[4] Yang R, Kameda H, Takada S. Shell model FEM analysis of buried pipelines under seismic loading (1988). Bull Disaster Prev Res Inst 1988;38(3):115–46.
[5] Kuwata Y, Takada S. Seismic risk assessment and upgrade strategy of hospital-lifeline performance. Sixth U.S. Conference and workshop on lifeline earthquake engineering (TCLEE) 2003, Aug, 10-13, Long Beach, California, US. 2003.
[6] Takada S, Yasuo O. Seismic monitoring and real time damage estimation for lifelines Technical Report, Report No: CONF-9508226-ISBN 0-7844-0101-2; TRN: IM9651%%475 1996.
[7] Takada S, Hassani N, Fukuda K. A new proposal for simplified design of buried steel pipes crossing active faults. J Earthq Eng Struct Dyn 2001;30(8):1243–57https://doi.org/10.1002/eqe.62.
[8] Takada S, Liang J, Li T. Shell-mode response of buried pipelines to large fault movements. J Struct Eng 1988;44A.
[9] Nourzadeh D, Takada S. Response of gas distribution pipeline network to seismic wave propagation in Greater Tehran Area. Iran. Sixth China-Japan-US trilateral symposium on lifeline earthquake engineering, May28-June 1. 2013. Chengdu, China.
[10] Javanbarg M, Takada S. © 2010 FurutaFrangopolShinozukaeditors. Seismic reliability assessment of water supply systems. Safety, reliability and risk of structures, infrastructures and engineering systems. London: Taylor & Francis Group978-0-415-47557-0; 2013.
[11] O'Rourke TD, Grigoriu MD, Khater MM. Sundarajan C, editor. Seismic response of buried pipes. pressure vessel and piping technology – a decade of progress. vol. 1985. ASME; 1985. p. 281–323.
[12] O'Rourke TD, Gowdy TE, Stewart HE, Pease JW. Lifeline and geotechnical aspects of the 1989 Loca Prieta earthquake. Proceedings of the 2nd international conference on recent advances in geotechnical engineering and soil dynamics. RoUa, Mo: University of Missouri-Rolla; 1991. p. 1601–12.
[13] O'Rourke TD, Pease JW, Stewart HE. Lifeline performance and ground deformation during the earthquake. The lomo Prieta, California, earthquake of October 17. 1989. Marina District. 1992.
[14] O'Rourke TD, Bonneau AL, Pease JW, Shi P, Wang Y. Liquefaction and ground failures in San Francisco. Earthq Spectra 2006;22(S2):S91–112.
[15] Toshima T, Iwamoto T, Nakajima T. Study on behavior of buried pipes in liquefied ground. 12th world conference on earthquake engineering, Auckland, New Zealand, 2000. 2000.
[16] Maltby TC, Calladine CR. An investigation into upheaval buckling of buried pipelines–I. Experimental apparatus and some observations. Int J Mech ScL 1995;37(1995):943.
[17] Maltby TC, Calladine CR. An investigation into upheaval buckling of buried pipelines–II. Theory and analysis of experimental observations. Int J Mech ScL 1995;37(1995):965.
[18] Towhata I, Tokida K, Tamari Y, Matsumoto H, Yamada K. Prediction of Permanent Lateral Displacement of Liquefied Ground by Means of Variational Principle National Centre for Earthquake Engineering Research; 1991. Technical Report NCEER-91-0001.
[19] Technical Report, NCEER-92-0002 O'Rourke TD, Hamada M, editors. Case studies of liquefaction and lifeline performance during past earthquakes. Buffalo, NY: National Center for Earthquake Engineering Research, State University of New York at Buffalo; 1992.
[20] O'Rourke TD, Jeon S-S, Toprak S, Cubrinovski M, Hughes M, Ballegooy SV, Bouziou D. Earthquake response of underground pipeline networks in Christchurch, NZ February 2014 Earthq Spectra 2014;30(1):183–204.
[21] Fuchida K, Shirinashihama S, Akiyshi T. Protection of buried pipelines from liquefaction by ground improvements. Eleventh world conference on earthquake engineering. 1996. Paper No. 583.
[22] Tavakoli Mehrjardi Gh, Moghaddas Tafreshi SN, Dawson AR. Combined use of geocell reinforcement and rubberesoil mixtures to improve performance of buried pipes. Geotext Geomembranes 2012;34(2012):116–30.
[23] Jahed Armaghani D, Faizi K, Hajihassani M, Tonnizam Mohamad E, Nazir R. Effects of soil reinforcement on uplift resistance of buried pipelines. Measurement 2015;64(2015):57–63.
[24] Faizi K, Jahed Armaghani D, Momeni E, Nazir R, Tonnizam Mohamad E. Uplift resistance of buried pipelines enhanced by geogrid (2014). Soil Mech Found Eng 2014;51(4):188–95https://doi.org/10.1007/s11204-014-9276-6.
[25] American Lifelines Alliance. Seismic Guidelines for Water Pipelines. National Institute of Building Science; 2005. G&E Report 80.01.01.
[26] Seed HB, Idriss IM. Simplified procedure for evaluating soil liquefaction potential. J Soil Mech Found Div, ASCE 1971;97(SM9):1249–73.
[27] Seed HB, Idriss IM. Ground motions and soil liquefaction during earthquakes. Oakland, CA: Earthquake Engineering Research Institute; 1982. p. 134.
[28] Seed HB, Tokimatsu K, Harder Jr. LF, Chung R. Influence of SPT procedures in soil liquefaction resistance evaluations. J Geotech Geoenviron Eng, ASCE 1985;111(12):1425–45.
[29] Youd T,L, Idriss IM. Liquefaction resistance of soils: summary report from the 1996 NCEER and 1998 NCEER/NSF workshops on evaluation of liquefaction resistance of soils. J Geotech Geoenviron Eng, ASCE 2001;127(4):297–313.
[30] lwasaki T, Tatsuoka F, Tokida K, Yasuda S. A practical method for assessing soil liquefaction potential based on case studies at various sites in Japan. Second international conference on mierozonation for safer construction research and application, 1978. 1978.
[31] Tatsuoka F, lwasaki T, Tokida K, Yasuda S, Hirose M, lmai T, Kon-no M. Standard penetration tests and soil liquefaction potential evaluation 1980 Soils Found 1980;20(4).
[32] lwasaki T, Tokida K. Soil liquefaction potential evaluation with use of the simplified procedure. Proc. International conference on recent advances in geotechnical earthquake engineering and soil dynamics, 1981. 1981.
[33] Iwasaki T, Arakawa T, Tokida K. Simplified procedures for assessing soil liquefaction during earthquakes. Proceedings of soil dynamics and earthquake engineering conference, Southampton, UK, 1982. 1982.
[34] Japan Gas Association. Seismic design guideline for liquefaction for high pressure gas pipeline. 2001. JGA-207-01 (In Japanese).
[35] Japan Gas Association (JGA). Seismic design guideline for high pressure has pipelines. 2000. In Japanese.
[36] Japan Gas Association (JGA). Seismic design guideline for middle and low pressure gas pipelines. 2003. In Japanese.
[37] American Lifeline Alliances (ALA). Guidelines for design of buried steel pipes. USA: ASCE; 2001.
[38] Gholipour Y., Bozorgnia Y., Rahnama M., Berberian M., Ghoreishi, M., Talebian, Nazari, Shoja Taheri J., Shafie, A. Probabilistic seismic hazard analysis: phase I - Greater Tehran region. School of Engineering, University of Tehran. Seismic Hazard Analysis Research of I.R.Iran Phase I-Greater Tehran Region.
[39] Klügel JU, Mualchin L, Panza GF. A scenario-based procedure for seismic risk analysis. J Eng Geol 2006;88:1–22. Elsevier.
[40] Ashtari M, Hatzfeld D, Kamalian N. Microseismicity in the region of Tehran. J Tectonophysics 2005;395:193–208. Elsevier.
[41] Japan International Cooperation Agency (JICA). The study on seismic microzoning of the Greater Tehran Area in the Islamic Republic of Iran. 2000.
[42] Kamae K, Irikura K, Pitarka A. A technique for simulating strong ground motion using hybrid green's function. Bull Seismol Soc Am 1998;88(2):357–67.
[43] Irikura K, Miyake H, Iwata T, Kamae K, Kawabe H. Revised recipe for predicting strong motion and its validation. Proceedings of the 11th Japan Earthquake Engineering Symposium. 2002. p. 567–72.
[44] Mir Hosseini SM, Kari M. Preliminary microzoning of areas prone to liquefaction in Tehran. Proceedings of second international conference on Seismology and earthquake engineering, Iran. 1993.
[45] Mir Hosseini SM. Microzonation of southeast part of Tehran to liquefaction. Eleventh world conference on earthquake engineering. 1996. Paper No. 1723.
[46] Mir Hosseini SM, Komak Panah A, Esmaeeli AM, Aref Pour B, Ghasemi A. Microzonation for liquefaction in southern part of Tehran. Iran: National Research Program in IIEES; 2002.
[47] Askari F, Kasaei M. Analysis of liquefaction potential in some parts of southeast Tehran. J Fac Eng Univ Tokyo. Electron. J. Geotech. Eng. 2003;9. Iran.
[48] Pezeshki H, Ueno J, Takada S. Performance and allowable fault dislocation for steel and polyethylene pipelines crossing faults. Mem Constr Eng Res Inst 2004;46:152–63.
[49] Towhata I. Geotechnical earthquake engineering. Springer978-3-540-35782-7; 2008.
[50] Ishihara K. Soil behaviour in earthquake geotechnics. Oxford University Press0-19-856224-1; 1996.